Stem Cell Reports
Article

ISSCR

OPEN ACCESS

Bone Size and Quality Regulation: Concerted Actions of mTOR in Mesenchymal Stromal Cells and Osteoclasts

Hongguang Wu,[1,2,8] Zhixiang Wu,[1,2,8] Ping Li,[2] Qian Cong,[2] Rongrong Chen,[3] Wenrui Xu,[4] Soma Biswas,[2] Huijuan Liu,[1,2] Xuechun Xia,[2] Shanshan Li,[5] Weiwei Hu,[5] Zhenlin Zhang,[5] Samy L. Habib,[6] Lingli Zhang,[7] Jun Zou,[7] Hongbing Zhang,[3] Weihong Zhang,[4,*] and Baojie Li[1,2,7,*]

[1]Bio-X-Renji Hospital Research Center, Renji Hospital, School of Medicine, Shanghai Jiao Tong University, Shanghai 200127, China
[2]Key Laboratory for the Genetics of Developmental and Neuropsychiatric Disorders, Bio-X Institutes, Ministry of Education, Shanghai Jiao Tong University, Shanghai 200240, China
[3]State Key Laboratory of Medical Molecular Biology, Department of Physiology, Institute of Basic Medical Sciences
[4]Department of Radiology
Peking Union Medical College and Chinese Academy of Medical Sciences, Beijing 100730, China
[5]Research Unit, Department of Osteoporosis and Bone Diseases, Shanghai Jiao Tong University Affiliated with Sixth People's Hospital, 600 Yishan Road, Shanghai 200233, China
[6]Department of Cellular and Structural Biology, South Texas Veterans Health Care System, San Antonio, University of Texas Health Science Center at San Antonio, San Antonio, TX 78229, USA
[7]Scientific Research Department, Shanghai University of Sport, 399 Changhai Road, Yangpu District, Shanghai, 200438, China
[8]Co-first author
*Correspondence: zhangweihong@pumch.cn (W.Z.), libj@sjtu.edu.cn (B.L.)
http://dx.doi.org/10.1016/j.stemcr.2017.04.005

SUMMARY

The bone size and quality, acquired during adolescent growth under the influence of anabolic hormones, growth factors, and nutrients, determine the height and bone stability and forecast osteoporosis risks in late life. Yet bone size and quality control mechanisms remain enigmatic. To study the roles of mammalian target of rapamycin (mTOR) signaling, sensor of growth factors and nutrients, in bone size and quality regulation, we ablated *Tsc1*, a suppressor of mTOR, in mesenchymal stromal cells (MSCs), monocytes, or their progenies osteoblasts and osteoclasts. mTOR activation in MSCs, but much less in osteoblasts, increased bone width and mass due to MSC hyperproliferation, but decreased bone length and mineral contents due to defective MSC differentiation. mTOR activation promotes bone mineral accretion by inhibiting osteoclast differentiation and activity directly or via coupling with MSCs. Tuberous sclerosis complex patient studies confirmed these findings. Thus, mTOR regulates bone size via MSCs and bone quality by suppressing catabolic activities of osteoclasts.

INTRODUCTION

The organ size, determined by the number and size of cells in the organ, is regulated by genetic and environmental factors (Csibi and Blenis, 2012; Penzo-Mendez and Stanger, 2015). The size of bones determines the height, build, and stability of the skeleton, while the quality of bones, defined by bone matrix and mineral contents and microstructures, determines the bone strength (Whiting et al., 2004). It is estimated that peak bone mass accounts for 60% of the risk of osteoporosis (Baxter-Jones et al., 2011). The maximal bone size, mass, and strength are reached in humans at the age of 23–24 years and in mice at 10–12 weeks (Bonjour and Chevalley, 2014; Farr and Khosla, 2015). Bone growth and remodeling are carried out by coordinated osteoblastic bone formation and osteoclastic bone resorption (Henriksen et al., 2014; Karsenty et al., 2009). Osteoblasts (OBs) are derived from bone marrow-mesenchymal stromal cells (BM-MSCs), which can self-renew and differentiate into OBs, chondrocytes, or adipocytes, whereas osteoclasts (OCs) are derived from monocytes (Edwards and Mundy, 2011; Harada and Rodan, 2003; Lacey et al., 2012). Proliferation of stem cells and progenitors increases the pool of OBs or OCs, while proper maturation determines the activities of these cells. Bone size, mass, and quality can be regulated by the growth hormone-insulin growth factor (IGF) axis, nutrition, steroid hormones, vitamin D, and mechanical stimuli (Bonjour and Chevalley, 2014; Hendrickx et al., 2015; Rosello-Diez and Joyner, 2015; Zemel, 2013). It is generally believed that IGFs promote OB and chondrocyte proliferation and differentiation, which mediate the anabolic effects of IGFs on bone growth (Callewaert et al., 2010; Canalis, 2009; Yakar et al., 2010).

The mammalian target of rapamycin (mTOR) pathway is the sensor of growth factors, including IGF1, macrophage colony-stimulating factor (M-CSF), and nutrients (Hay and Sonenberg, 2004; Laplante and Sabatini, 2012), and is expected to play critical roles in bone growth spurt during adolescence. Activated mTOR increases global protein synthesis to promote cell proliferation (Jewell et al., 2013; Johnson et al., 2013). In humans, tuberous sclerosis complex (TSC) patients carry mutations in one allele of *TSC1* or *TSC2*, encoding negative regulators of mTOR, and they develop benign tumors in multiple organs due to loss of heterozygosity of the *TSC* genes (Laplante and Sabatini,

2012). In addition, TSC patients develop focal sclerotic bone lesions (Avila et al., 2010; Li et al., 2015; Rafal et al., 2013; Umeoka et al., 2008). In mouse, *mTor* ablation or mTOR activation by ablation of *Tsc1* or *Tsc2* causes embryonic or neonatal lethality (Laplante and Sabatini, 2012). Studies of mice with *Tsc1* or *Tsc2* deleted in committed OBs or chondrocytes established roles for mTOR signaling in bone mass accrual and endochondral ossification (Huang et al., 2015; Riddle et al., 2014), with the cartilage studies being limited to embryos or newborns due to survival problems of the mice (Chen and Long, 2014; Yan et al., 2016). Yet, the roles for mTOR signaling in bone size and quality control during adolescent growth, especially from the angle of the stem cells of the skeleton, remain largely unknown.

Here, we ablated *Tsc1* in BM-MSCs and monocytes, as well as in their progenies, OBs and OCs, and found that mTOR regulates bone size in length and width by coordinating MSC proliferation and differentiation, and bone quality by suppressing osteoclastogenesis and bone resorption in cell-autonomous manners and by regulating the expression of OPG and RANKL by MSCs. The bone phenotypes induced by *Tsc1* ablation mediated by *Prx1-Cre* or *LysM-Cre* were largely rescued by treatment with rapamycin, an mTOR inhibitor. Analysis of the TSC patients from the Han Chinese population revealed that more than 90% of the patients show increased focal bone density, which is associated with a decrease in bone resorption marker and an increase in bone formation marker. These findings thus uncover multifaceted roles for mTOR signaling in regulating bone size and quality, and underscore the decisive contribution of suppression of bone resorption to the achievement of peak bone mineral contents.

RESULTS

The mTOR Pathway Was Activated in Multiple Locations of the Bone during Adolescent Growth

mTOR can be activated by growth factors and nutrients. We found that in femurs of 1-day-old, 4-week-old, or 8-week-old mice, mTOR activation, manifested by S6 phosphorylation, was detectable in the proliferation and prehypertrophic zones of the growth plate (Figures 1A–1C), which are involved in longitudinal bone growth, the region underneath the growth plate, where trabecular bones are formed, and the periosteal and endosteal surfaces, which are responsible for bone radial growth (Figures 1A–1C). Staining of both p-S6 and Col2 or Osx confirmed that mTOR activation occurred in chondrocytes and OBs (Figure S1A). p-S6 signals were reduced in 8-week-old mouse bones compared with those in 1-day-old and 4-week-old mice, suggesting that mTOR is highly activated during adolescent growth. Moreover, starvation inhibited mTOR activation, whereas feeding activated mTOR on mouse bone sections (Figures 1D–1F), confirming that food intake or nutrients can activate mTOR in the bone.

Prx1-Cre; Tsc1$^{f/f}$ Mice Showed Shorter and Thicker Long Bones and Joint Defects

It has been reported that *mTor* ablation in BM-MSCs causes mouse neonatal lethality (Chen and Long, 2014). To further test the physiological function of mTOR activation in bone growth, we deleted *Tsc1* in BM-MSCs by crossing floxed *Tsc1* mice with *Prx1-Cre* mice (Figure S1B) (Logan et al., 2002; Meikle et al., 2007). Our previous studies have confirmed that Prx1 marks stromal cells with tri-lineage differentiation potentials and labels cells at the growth plate, trabecular region, and periosteal surface (Cong et al., 2016). Western blot and immunohistochemical analysis confirmed that *Tsc1* was largely deleted in BM-MSC cultures and on bone sections, leading to an increase in p-S6 (Figures S1C and S1D). The *Tsc1*-deficient mice were born at the expected Mendelian ratio and showed unaltered body weight and length compared with wild-type (WT) littermates (Figure S1E).

Micro-computed tomography (CT) analysis showed that the length of the long bones of the *Tsc1*-deficient mice was decreased compared with control littermates of the same gender at 2.5 months of age (Figures 2A and 2B), when peak bone mass is achieved in mice. Histological analysis revealed that the mutant mice showed an increase in the height of growth plates and the size of chondrocytes compared with control mice (Figure 2C). The chondrocyte proliferation zone and hypertrophy zone were not clearly separated in the mutant mice (Figure 2C), likely due to disruption of the coordination between chondrocyte proliferation and differentiation. The mutant mice also showed a defect in articular cartilage and joint formation (Figure 2D). A similar perichondrium and cartilage anomaly has been reported in hereditary multiple exostoses patients, a disorder caused by mutations in *EXT1* and *EXT2* (Huegel et al., 2013; Jones et al., 2010), yet we found that mTOR activation did not alter the protein levels of EXT1 or EXT2 in MSCs, chondrocytes, or cartilage (Figures S2A–S2C).

On the other hand, the mutant mice showed an increase in the width of femurs and physeal growth plate (Figures 2A, 2E, and 2F). It is believed that, in addition to periosteal bone apposition, the width of the growth plate is an important factor determining the width of long bones (Wang et al., 2011). These results indicate that TSC1 plays an important role in bone growth in both length and width, although in opposed ways.

It has been reported that TSC1 also activates mTOR-independent pathways such as RAF and NOTCH. We found that in BM-MSCs, *Tsc1* deletion did not affect the protein levels

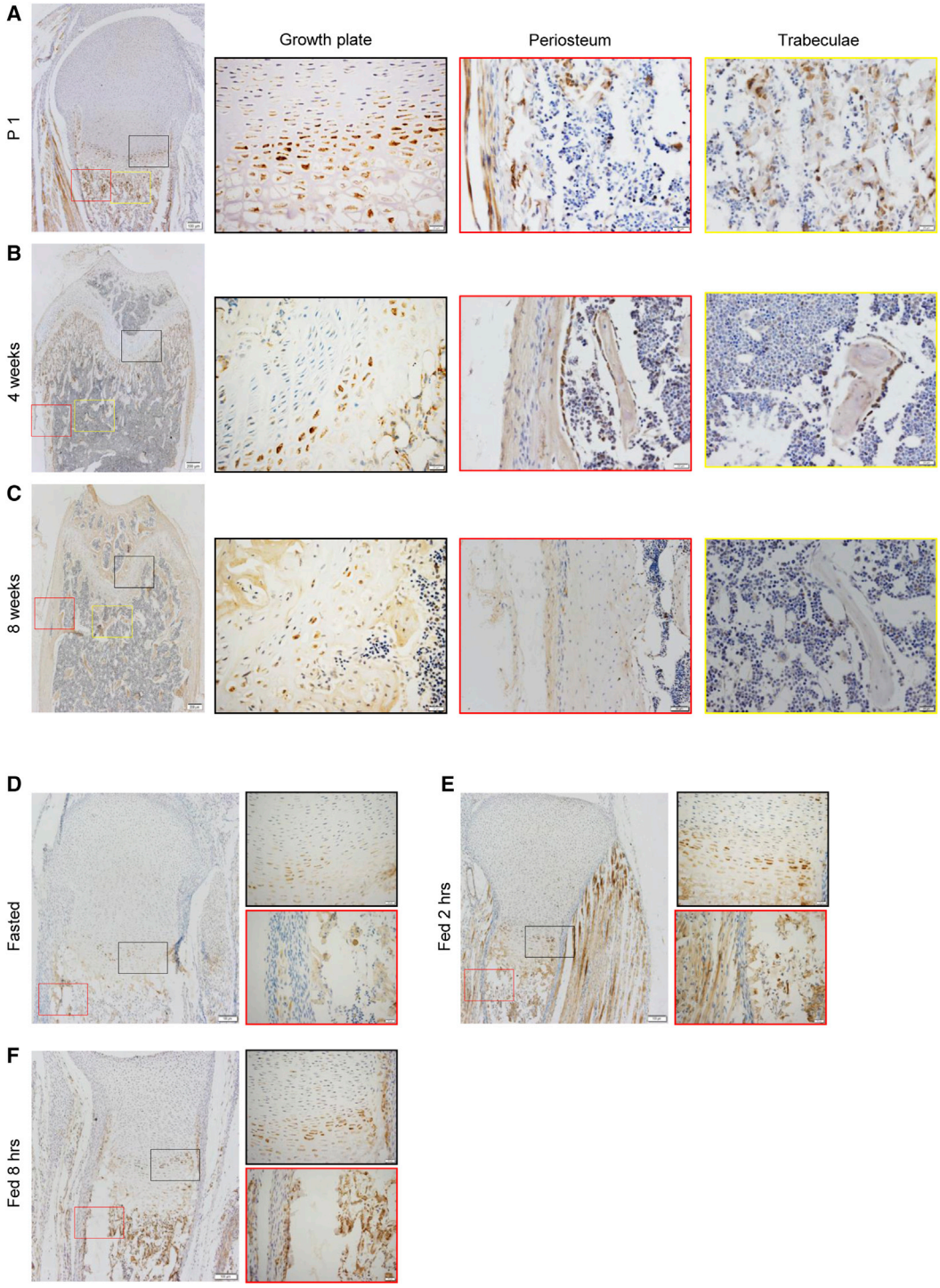

Figure 1. mTOR Was Activated in the Bone during Adolescent Growth and by Feeding

(A–C) Immuno-staining of p-S6 on bone sections of 1-day-old (A), 4-week-old (B), or 8-week-old mice (C). The femur bones were decalcified and embedded in paraffin. Antibodies against p-S6 and secondary antibodies conjugated with horseradish peroxidase were used to detect the signal.

(D–F) Starvation inhibited mTOR activation, whereas feeding activated mTOR on bone sections. P1 pups were starved overnight (D) by separating from the mother and then euthanized 2 hr (E) or 8 hr (F) after feeding. The femur bones were frozen sectioned and stained for p-S6. Scale bars, 200 μm (A–F left panels) and 50 μm (A–F right panels).

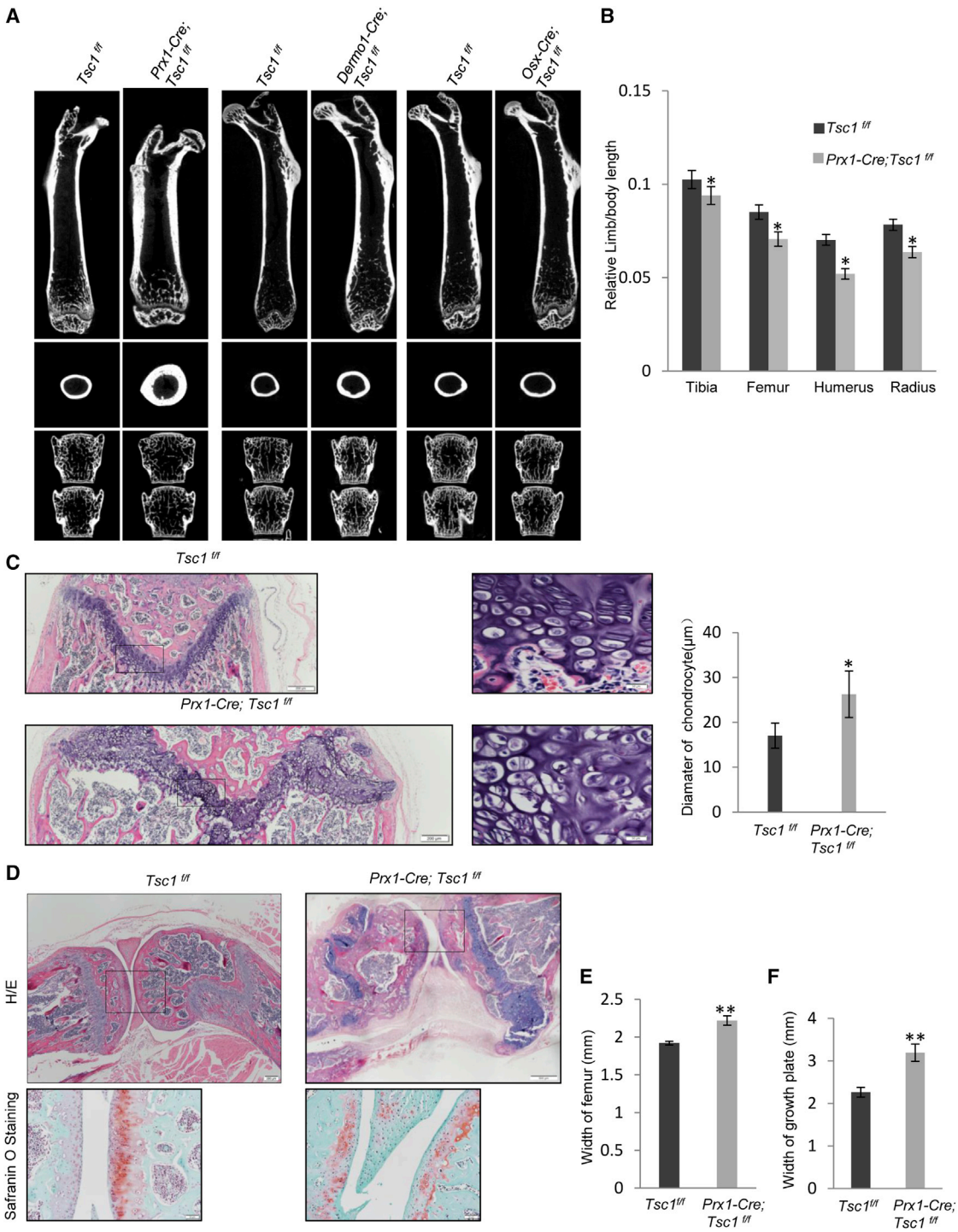

Figure 2. Ablation of *Tsc1* in *Prx1*+ MSCs but Not in *Dermo1*+ or *Osx*+ OBs Led to Shortened but Broadened Limbs and Joint Deformation

(A) Micro-CT images of the femur bones and the vertebrae (L3 and L4) of 2.5-month-old *Prx1-Cre; Tsc1*$^{f/f}$, *Dermo1-Cre; Tsc1*$^{f/f}$, and *Osx-Cre; Tsc1*$^{f/f}$ mice. Upper panel, coronal plane of femur; middle panel, transverse plane of femur; bottom panel, vertebrae.

(B) Quantitation data showed that the length of *Prx1-Cre; Tsc1*$^{f/f}$ mouse long bones was decreased compared with control mice. N = 15 mice.

(C) H&E staining of the growth plates of 2.5-month-old *Prx1-Cre; Tsc1*$^{f/f}$ and control mouse femur bones. Right panel: quantitation data of the diameter of chondrocytes. Scale bars, 200 μm (left panel) and 20 μm (middle panel). N = 3 mice (6 views each).

(legend continued on next page)

of RAF or the activation of its downstream ERK kinases (Figure S2D). *Tsc1* deficiency slightly increased the protein levels of NOTCH1 (Figure S2D), which may mediate the effect of mTOR activation on OB differentiation (Huang et al., 2015). To determine whether the skeletal phenotypes observed in *Prx1-Cre; Tsc1*$^{f/f}$ mice are caused by mTOR activation, we treated the mutant and control mice with rapamycin and found that rapamycin inhibited skeletal growth in WT mice (Figures S3A–S3M), as reported previously (Yan et al., 2016). Moreover, rapamycin largely rescued the skeletal phenotypes including bone width/length, bone mass, trabecular bone number, trabecular separation, the growth plate height, the size of chondrocytes, and the joint development anomaly in *Prx1-Cre; Tsc1*$^{f/f}$ mice (Figures S3A–S3M). These results indicate that mTOR signaling downstream of TSC1 deficiency plays an important role in bone growth.

The change in bone size and joint formation defects observed in *Prx1-Cre; Tsc1*$^{f/f}$ mice are not reported in mice with *Tsc1* or *Tsc2* ablated in OBs (Chen and Long, 2014; Huang et al., 2015; Riddle et al., 2014). Moreover, these defects were not obvious in *Prx1-Cre; Tsc1*$^{f/f}$ embryos or p1 newborn mice. The *Prx1-Cre; Tsc1*$^{f/f}$ embryonic skeletons (E18.5) appeared normal and the length of the long bones of day 1 pups was not significantly affected (Figures S4A and S4B). The p1 pups did not develop the joint problem either (Figure S4C). These results suggest that the bone size alteration and joint defects observed in *Prx1-Cre; Tsc1*$^{f/f}$ adult mice are developed during adolescent growth.

Prx1-Cre; Tsc1$^{f/f}$ Mice Showed Increased Bone Volume but Decreased Bone Mineralization

Micro-CT analyses revealed that the mutant mice showed an increase in the thickness of cortical bones and the volume and thickness of trabecular bones (Figures 3A–3C), accompanied by a decrease in the number of trabecular bones and bone separation (Figures 3D and 3E). Bone histomorphometry revealed that the 2.5-month-old mice showed an increase in bone formation rate but a decrease in bone mineralization rate (Figures 3F and 3G), suggesting that bone mineralization might be impeded even though bone formation is increased.

We found that the cortical bones appeared to have quality problems. Firstly, they were porous, accompanied by an increase in the number of blood vessels, as CD31, a marker for endothelial cells, could stain these pores (Figure 3H). Secondly, von Kossa staining and H&E staining showed that the mutant bone was rich in osteoids that were not fully mineralized (Figures 3I and 3J). The mineralization defects are similar to what have been reported in mice with *Tsc1* or *Tsc2* ablated in OBs, which were rescued by rapamycin treatment (Chen and Long, 2014; Huang et al., 2015; Riddle et al., 2014). Thirdly, the bones were more fragile than WT bones, based on three-point bending experiments (Figure 3K). These results, taken together, indicate that mTOR activation by ablation of *Tsc1* in *Prx1*+ MSCs inhibits bone mineralization, disrupts bone microstructure, and reduces bone strength, thus lowering the bone quality.

mTOR Activation Regulated Bone Size and Mass Mainly via MSCs but Not OBs

To determine the contributions of mTOR signaling in MSCs and OBs to the bone phenotypes observed in *Prx1-Cre; Tsc1*$^{f/f}$ mice, we ablated *Tsc1* in *Dermo1*+ MSCs and *Osx*+ OBs, respectively. Dermo1 is believed to be expressed in BM-MSCs after Prx1, while Osx is expressed in committed OBs after Runx2 (Figure S1B) (Rodda and McMahon, 2006; Yu et al., 2003). Western blot analysis of BM-MSCs and differentiated OB cultures confirmed that *Tsc1* was largely deleted, leading to an increase in p-S6 (Figure S4D). We found that these two mouse lines showed normal body weight and body length (Figures S4E and S4F).

X-ray imaging analyses revealed that unlike *Prx1-Cre; Tsc1*$^{f/f}$ mice, the length and the width of the femurs and the growth plates were not significantly altered in *Dermo1-Cre; Tsc1*$^{f/f}$ mice or *Osx-Cre; Tsc1*$^{f/f}$ mice compared with their control littermates (Figures 2A and S4G and data not shown). These two mouse lines showed an increase in trabecular bone volume and cortical bone thickness, with the increase in *Dermo1-Cre; Tsc1*$^{f/f}$ mice being greater than that in *Osx-Cre; Tsc1*$^{f/f}$ mice (Figures 3A, 3B, and S4H–S4J). The increase in trabecular bone volume and cortical bone thickness in these two mouse lines were much less than those of *Prx1-Cre; Tsc1*$^{f/f}$ mice (Figures 2A, 3A, and 3B). These results collectively suggest that mTOR signaling regulates trabecular and cortical bone mass mainly via MSCs.

We also compared the vertebrae (L3 and L4) of the three *Tsc1*-deficient mouse lines against their respective control littermates using micro-CT, and found that the bone

(D) H&E staining of the sections of the knee joint of *Prx1-Cre; Tsc1*$^{f/f}$ and control mice. Scale bars, 200 μm (upper panel) and 20 μm (lower panel).

(E) Quantitation data showed that the width of the *Prx1-Cre; Tsc1*$^{f/f}$ mouse femur bones was increased compared with control mice. N = 6 mice.

(F) Quantitation data showed that the width of growth plates of *Prx1-Cre; Tsc1*$^{f/f}$ mouse femur bones was increased compared with control mice. N = 6 mice.

Error bars represent the SD. *p < 0.05; **p < 0.01.

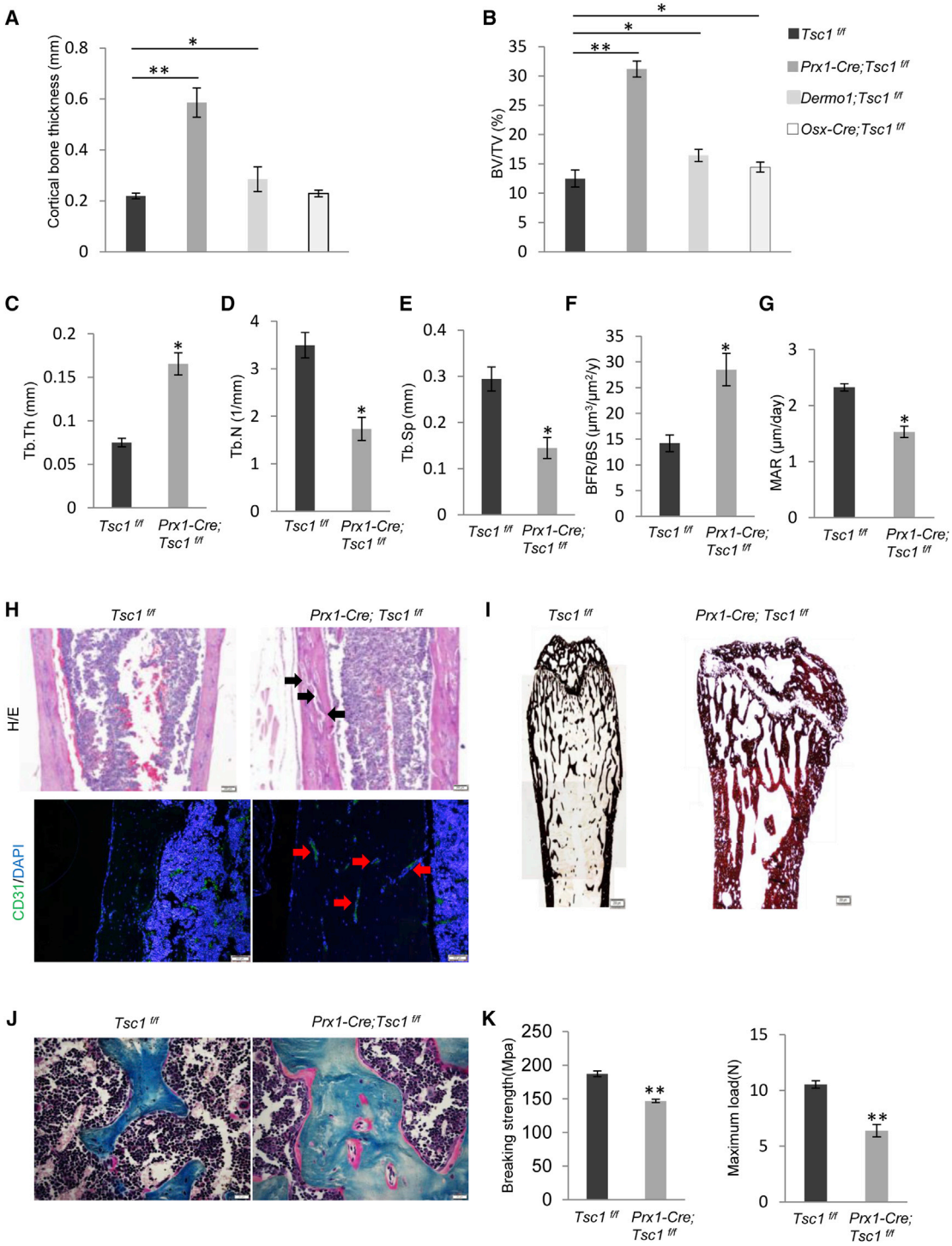

Figure 3. Ablation of *Tsc1* in MSCs Increased Bone Mass but Reduced Bone Quality

(A) Ablation of Tsc1 in *Prx1*+ MSCs increased the cortical thickness of femur bones to a greater extent than ablation of *Tsc1* in *Dermo1*+ or *Osx*+ OBs. N = 4 mice.

(B) Micro-CT analysis revealed that *Prx1-Cre; Tsc1$^{f/f}$* mice showed a greater increase in trabecular bone volume than *Dermo1-Cre; Tsc1$^{f/f}$* and *Osx-Cre; Tsc1$^{f/f}$* mice. N = 4 mice.

(legend continued on next page)

mineral contents were not significantly altered in *Prx1-Cre; Tsc1$^{f/f}$* mice or *Osx-Cre; Tsc1$^{f/f}$* mice, whereas *Dermo1-Cre; Tsc1$^{f/f}$* mice showed a modest increase in bone mineral contents (Figure 2A).

Tsc1 Deficiency Increased the BM-MSC Pool but Inhibited MSC Differentiation

We found that on bone sections of *Prx1-Cre; Tsc1$^{f/f}$* mice, the number of Ki67-positive cells was greatly increased in the growth plate (Figures 4A and S4H). The heights of the Ki67-positive proliferation zone and the Col10-positive hypertrophic zone were increased (Figure S4H), suggesting that the balance between proliferation and differentiation of chondrocyte progenitors were disrupted by *Tsc1* ablation. In addition, the number of OBs per bone surface was significantly increased (Figure 4B). *Prx1-Cre; Tsc1$^{f/f}$* mouse bone marrow also contained an increased number of colony-forming units, an indicator of the number of MSCs (Figure 4C), suggesting that the pool of MSCs was expanded.

Tsc1$^{-/-}$ BM-MSCs showed a defect in chondrogenic differentiation, manifested by a decrease in Alcian blue staining and expression of chondrocyte marker Sox9, a defect in OB differentiation, manifested by a decrease in the expression of ALP and OB markers such as *Runx2*, *Osx*, and *ColIα*, and mineralization, without affecting MSC adipogenesis (Figures 4D and 4E). Therefore, *Tsc1* deficiency disrupted the balance between MSC proliferation and differentiation.

A previous study has shown that depletion of *Tsc1* in differentiated chondrocyte by *Col2-Cre* led to a defect in chondrocyte differentiation (Yan et al., 2016), which was shown to be mediated by an altered PTHrP-IHH loop (Kronenberg, 2006; Lee et al., 1995). We also found that Tsc1 depletion resulted in an increase in the mRNA levels of *Pthrp*, but not *Ihh*, in MSCs (Figure S2E). Our results support the notion that mTOR regulates chondrocyte differentiation via PTHrP (Yan et al., 2016).

We also looked at the major signaling pathways that control MSC osteogenic differentiation and found that *Tsc1* deficiency in MSCs decreased β-catenin activation without significantly affecting the activation of Smad1/5/8 or p38 MAPK (Figures 4F and S2F). Since Wnt-β-catenin is a master regulator of OB differentiation, these results suggest that mTOR may regulate MSC osteogenic differentiation via compromising the Wnt-β-catenin pathway (Huang et al., 2015). We also checked the β-catenin-independent pathways activated by Wnt molecules such as Wnt5a (Yang et al., 2003; Gao et al., 2011), and found that *Tsc1* deletion led to a modest decrease in JNK activation, a downstream signaling molecule of Wnt5a, without affecting the expression of Wnt5a (Figures S2G and S2H). The effects of the non-canonical Wnt pathways warrant further investigation.

Ablation of *Tsc1* in MSCs but Not OBs Showed Suppressed Osteoclastogenesis and Bone Resorption

We then stained for TRAP-positive OCs on femur bones and found that *Prx1-Cre; Tsc1$^{f/f}$* mice showed a decreased number of OCs (Figure 5A). Bone histomorphometry analysis confirmed that the mutant mice showed a decrease in bone erosion surface and the number of OCs, which were rescued by rapamycin treatment (Figures 5B and 5C and data not shown). Furthermore, *Prx1-Cre; Tsc1$^{f/f}$* mice showed a decrease in urine deoxypyridinoline (DPD) levels, an in vivo bone resorption marker (Figure 5D). On the other hand, *Dermo1-Cre; Tsc1$^{f/f}$* and *Osx-Cre; Tsc1$^{f/f}$* mouse lines did not show a change in the number of TRAP-positive OCs (Figure 5A). These results indicate that *Tsc1* deficiency in MSCs, but not in OBs, suppresses osteoclastogenesis, which may help to promote bone mineral accrual.

To understand how mTOR signaling regulates the coupling between MSCs and osteoclastogenesis, we analyzed the mRNA levels of *Rankl*, *Opg*, and *M-Csf* in *Tsc1$^{-/-}$* and control BM-MSCs and found that *Tsc1* deficiency greatly increased the expression of *Opg* and decreased the expression of *Rankl* (Figure 5E). Similar results were obtained from immuno-staining for RNAKL and OPG on bone sections and measurement of RANKL and OPG in the bone marrow (Figures S5A and S5B). These results suggest that mTOR in BM-MSCs might regulate OPG and RANKL expression to suppress osteoclastogenesis and bone resorption. In addition, *M-Csf* expression was upregulated in *Tsc1*-deficient MSCs (Figure 5E). We showed that decreased M-CSF production by MSCs compromised proliferation of OC progenitor cells in co-culture experiments (Figure S5C).

(C–G) *Prx1-Cre; Tsc1$^{f/f}$* mice showed an increase in thickness (C) and the number (D), and a decrease in separation (E) of trabecular bones, and an increase in bone formation rate (BFR) (F) and mineral apposition rate (MAR) (G). N = 4 mice.
(H) *Prx1-Cre; Tsc1$^{f/f}$* mice femur cortical bones appeared to be porous, some of which were stained positive for CD31. Black arrow, pores; red arrow, blood vessel. Scale bars, 200 μm (upper panel) and 50 μm (lower panel).
(I) von Kossa staining of *Prx1-Cre; Tsc1$^{f/f}$* and control littermates showed that the mineralization was impeded in the mutant mouse bones. Scale bar, 200 μm.
(J) Masson staining of *Prx1-Cre; Tsc1$^{f/f}$* and control littermates showed that the mineralization was impeded in the mutant mouse bones. Scale bar, 50 μm.
(K) *Prx1-Cre; Tsc1$^{f/f}$* mice showed reduced bone strength, judged by the three-point bending experiment results. N = 4 mice.
Error bars represent the SD. *p < 0.05; **p < 0.01.

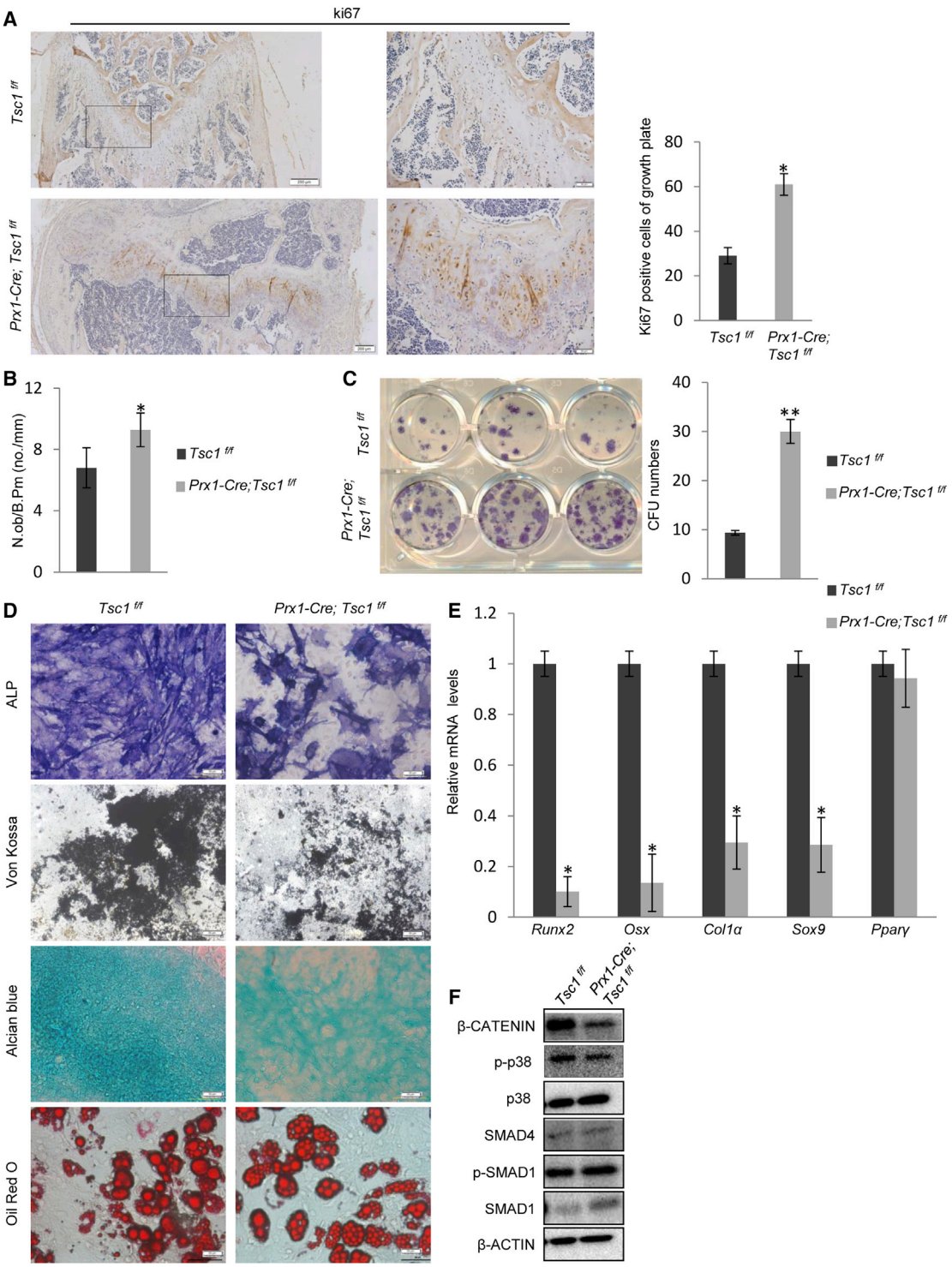

Figure 4. *Tsc1*$^{-/-}$ MSCs Showed Increased Proliferation, but Defective Osteogenic and Chondrogenic Differentiation

(A) Ki67 staining of femur bones of *Prx1-Cre; Tsc1*$^{f/f}$ and control mice. Right panel: quantitation data. Scale bars, 200 μm (left panel) and 50 μm (middle panel). N = 3 mice (6 views each).

(B) *Prx1-Cre; Tsc1*$^{f/f}$ mice showed an increase in the number of OBs in the trabecular region. N = 8 mice.

(C) *Prx1-Cre; Tsc1*$^{f/f}$ mice showed an increase in the number of bone marrow colony-forming units (CFU). Right panel: quantitation data. N = 4 independent experiments.

(legend continued on next page)

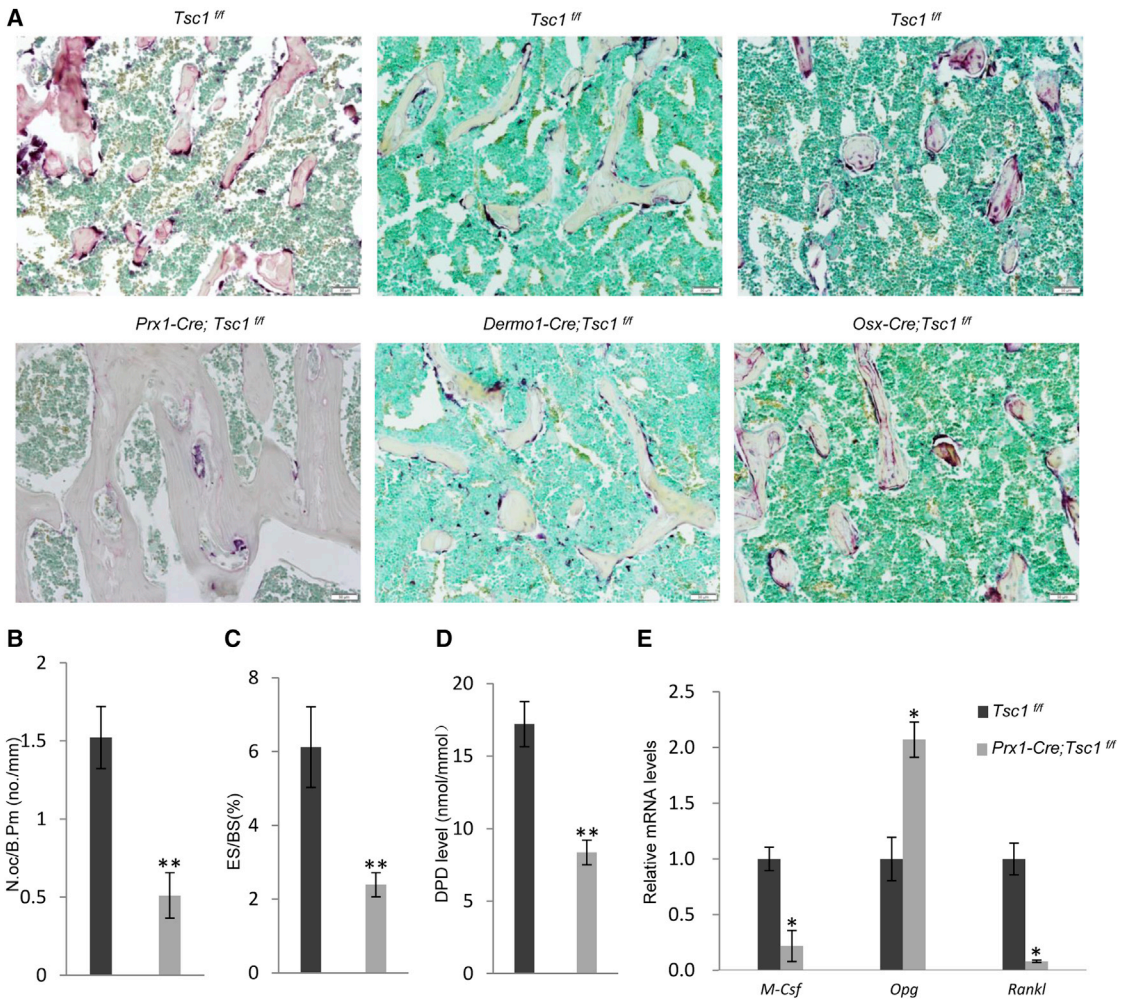

Figure 5. Ablation of *Tsc1* in *Prx1*+ MSCs but Not in *Dermo1*+ or *Osx*+ OBs Suppressed Osteoclastogenesis and Bone Resorption

(A) TRAP staining of bone sections revealed that femurs of *Prx1-Cre; Tsc1*$^{f/f}$ mice, but not *Dermo1-Cre; Tsc1*$^{f/f}$ or *Osx-Cre; Tsc1*$^{f/f}$ mice showed a decrease in the number of OCs in vivo. Scale bar, 50 μm. Data are from three independent experiments.

(B–D) *Prx1-Cre; Tsc1*$^{f/f}$ mice showed a decrease in bone erosion surface (B) (N = 8 mice), the number of OCs (C) (N = 8 mice), and the levels of urine DPD (D) (N = 4 mice).

(E) *Tsc1*$^{-/-}$ MSCs showed altered expression of *Rankl*, *M-Csf*, and *Opg*. N = 4 independent experiments.

Error bars represent the SD. *p < 0.05; **p < 0.01.

Ablation of *Tsc1* in Monocytes or OCs Increased Bone Mineral Contents

The above studies showed that mTOR signaling in MSCs regulated bone growth in size and volume via MSCs and that *Tsc1* deletion in MSCs also led to a decrease in bone mineralization. Although mTOR activation in MSCs regulates the expression of OPG and RANKL to suppress bone resorption and increase bone mineral contents, this turns out to be inadequate to keep up with bone growth in size.

(D) *Prx1-Cre; Tsc1*$^{f/f}$ BM-MSCs showed a decrease in OB differentiation, judged by ALP and von Kossa staining, a decrease in chondrocyte differentiation, judged by Alcian blue staining, but normal adipocyte differentiation. Scale bar, 100 μm.

(E) qPCR results revealed that *Tsc1*$^{-/-}$ MSCs showed a decrease in the expression of osteogenic and chondrogenic markers. N = 4 independent experiments.

(F) *Tsc1*$^{-/-}$ MSCs showed decreased activation of β-catenin. BM-MSCs were isolated from *Prx1-Cre; Tsc1*$^{f/f}$ and control mice, cultured for 3 days, and then harvested for western blot analysis.

Error bars represent the SD. *p < 0.05; **p < 0.01.

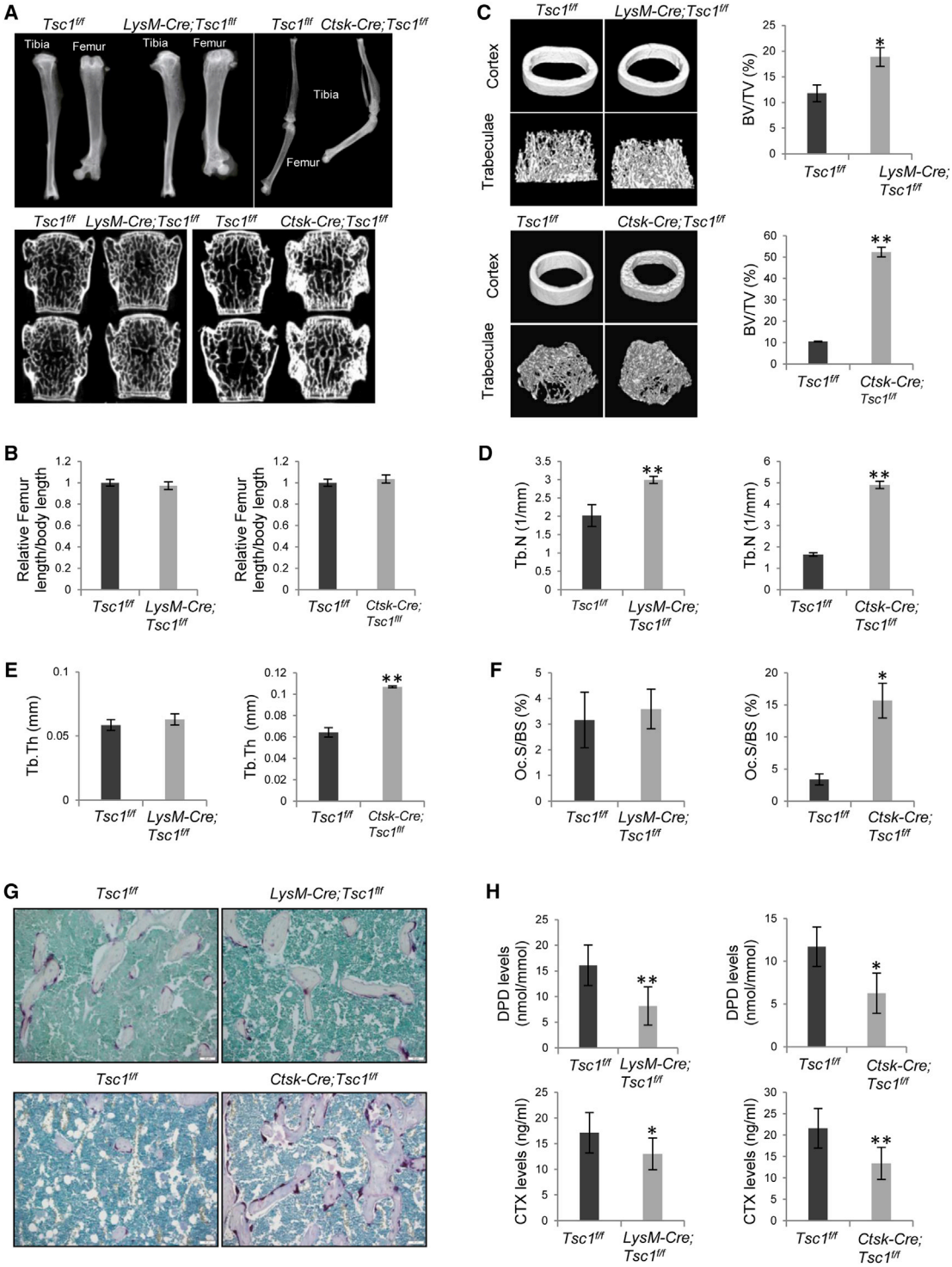

Figure 6. Ablation of *Tsc1* in *LysM+* Monocytes or *Ctsk+* OCs Led to a Decrease in Bone Resorption

(A) Micro-CT images of the femur bones and the vertebrae (L3 and L4) of *LysM-Cre; Tsc1$^{f/f}$* mice, *Ctsk-Cre; Tsc1$^{f/f}$* mice, and their respective control mice. N = 3 mice.

(B) The length of femur bones of *LysM-Cre; Tsc1$^{f/f}$* mice (left panel) and *Ctsk-Cre;Tsc1$^{f/f}$* mice (right panel) were not altered compared with those of control mice. N = 6 mice.

(legend continued on next page)

We then ablated *Tsc1* in monocytes, the OC progenitors, using *LysM-Cre* mice (Figure S1B) (Clausen et al., 1999), to test whether mTOR signaling in monocytes might affect adolescent bone mineral content accretion (Figure S6A). The mutant mice were born at the Mendelian ratio and they had unaltered body weight, body length, and femur radius and length (Figures 6A and 6B and data not shown).

Micro-CT analyses revealed that the mutant mouse femur displayed an increase in trabecular bone mass (Figures 6A–6E). The osteopetrotic phenotypes were largely rescued by inhibition of mTORC1 with rapamycin (Figures 6C and S6B). Bone histomorphometry analysis confirmed these findings and revealed that *LysM-Cre; Tsc1*$^{f/f}$ mice exhibited normal bone formation rate, bone mineralization rate, and the numbers of OCs in vivo (Figure 6F and data not shown). TRAP staining of bone sections confirmed that the numbers of OCs were similar between *LysM-Cre; Tsc1*$^{f/f}$ and control mice (Figure 6G). However, *LysM-Cre; Tsc1*$^{f/f}$ mice showed a decrease in bone resorption, demonstrated by a decrease in the serum levels of C-terminal telopeptide (CTX) and urine levels of DPD, two in vivo bone resorption markers (Figure 6H).

We then ablated *Tsc1* in differentiated OCs using *Ctsk-Cre* mice. These mice showed normal body weight and size and femur length (Figure 6B and data not shown), with an increase in trabecular bone volume and bone mineral contents (Figures 6C–6E). The osteopetrotic bone phenotypes in the *Ctsk-Cre; Tsc1*$^{f/f}$ mice were more severe than those of *LysM-Cre; Tsc1*$^{f/f}$ mice.

Surprisingly, the *Ctsk-Cre; Tsc1*$^{f/f}$ mice showed an increase in the number of OCs (Figure 6F), which was confirmed by TRAP staining on bone sections (Figure 6G). However, the levels of urine DPD and serum CTX were decreased (Figure 6H), suggesting that OCs might be functionally incompetent. On the other hand, bone formation rate and bone mineralization rate were not altered in *Ctsk-Cre; Tsc1*$^{f/f}$ mice (data not shown).

We also compared the vertebrae (L3 and L4) of *LysM-Cre; Tsc1*$^{f/f}$ and *Ctsk-Cre; Tsc1*$^{f/f}$ mouse lines against their respective control littermates using micro-CT, and found that bone mineral contents were not significantly altered in *LysM-Cre; Tsc1*$^{f/f}$ mice, similar to the femur bone phenotypes (Figure 6A). However, the *Ctsk-Cre; Tsc1*$^{f/f}$ mice showed greatly increased bone mineral contents (Figure 6A).

mTOR Activation Inhibited OC Differentiation, Fusion, and Activity

To determine the cellular basis of the decrease in bone resorption in *LysM-Cre; Tsc1*$^{f/f}$ mice, we isolated bone marrow monocytes and carried out in vitro differentiation assays. mTOR was activated in monocyte cultures, yet its activation went down once undergoing differentiation (Figure S7A). It was found that *Tsc1*$^{-/-}$ monocytes showed increased proliferation rates (Figure 7A). Yet, in response to RANKL and M-CSF, the formation of TRAP-positive OCs and the expression of mature OC markers were decreased, while the number of TRAP-positive mononuclear cells was increased (Figures 7B and 7C). The OCs derived from *Tsc1*$^{-/-}$ progenitors showed much fewer nuclei than WT OCs (Figures 7C and S7B), accompanied by reduced levels of *DC-Stamp* and *OC-Stamp* (Figure 7D), which are required for OC fusion (Helming and Gordon, 2009). Moreover, differentiated osteoclasts derived from *Tsc1*-deficient monocytes showed a decrease in resorption activity on bone chips, which was associated with a decrease in the expression of enzymes involved in bone resorption (Figures 7D and 7E). These results suggest that mTOR activation inhibits osteoclast differentiation, fusion, and function, but promotes proliferation. As such, compromised differentiation may even increase the proliferation of OC progenitors. This may explain why the number of OC numbers in vivo was not significantly altered in *LysM-Cre; Tsc1*$^{f/f}$ mice.

To further understand how mTOR activation affects OC differentiation, we looked at the signaling pathways known to control osteoclastogenesis. Western blot results showed that *Tsc1* deficiency led to a decrease in activation

(C) *LysM-Cre; Tsc1*$^{f/f}$ mice (upper panel) and *Ctsk-Cre; Tsc1*$^{f/f}$ mice (lower panel) showed an increase in the trabecular bone volume. Right panel: quantitation data. N = 4 mice.
(D) *LysM-Cre; Tsc1*$^{f/f}$ mice (left panel) and *Ctsk-Cre; Tsc1*$^{f/f}$ mice (right panel) showed an increase in the number of trabecular bones. N = 4 mice.
(E) *LysM-Cre; Tsc1*$^{f/f}$ mice (left panel) showed normal trabecular thickness, whereas *Ctsk-Cre; Tsc1*$^{f/f}$ mice (right panel) showed an increase in the thickness of trabecular bones. N = 4 mice.
(F) *LysM-Cre; Tsc1*$^{f/f}$ mice (left panel) showed normal numbers of OCs, whereas *Ctsk-Cre;Tsc1*$^{f/f}$ mice (right panel) showed an increase in the numbers of OCs. N = 6 mice.
(G) TRAP staining on bone sections revealed that femurs of *LysM-Cre; Tsc1*$^{f/f}$ mice showed normal number of TRAP-positive cells, whereas *Ctsk-Cre; Tsc1*$^{f/f}$ mice showed an increase in the number of TRAP-positive cells. Scale bar, 50 μm.
(H) *LysM-Cre;Tsc1*$^{f/f}$ and *Ctsk-Cre;Tsc1*$^{f/f}$ mice showed a decrease in the levels of urine DPD levels (upper panel) and serum levels of CTX (upper panel). N = 6 mice.
Error bars represent the SD. *p < 0.05; **p < 0.01.

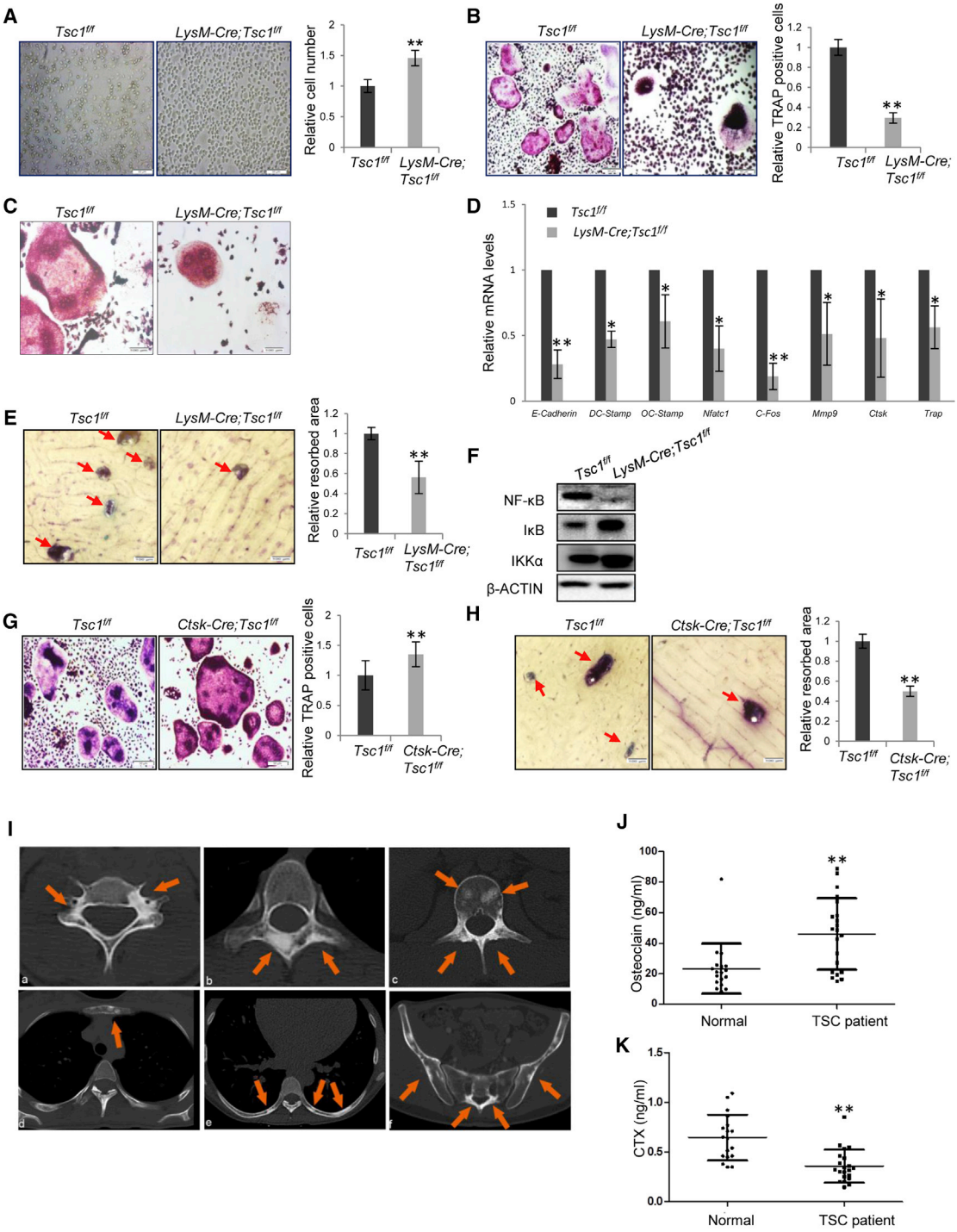

Figure 7. mTOR Activation Suppressed OC Differentiation, Fusion, and Resorption Activity, but Enhanced Proliferation

(A) Monocytes isolated from *LysM-Cre; Tsc1$^{f/f}$* mice showed an increase in proliferation. The monocytes isolated from *WT* and *LysM-Cre; Tsc1$^{f/f}$* mice were cultured for 3 days in the presence of M-CSF and RANKL. Scale bar, 50 μm. Right panel: quantitation data. N = 4 independent experiments.

(B) Ex vivo differentiation assays revealed that monocytes isolated from *LysM-Cre; Tsc1$^{f/f}$* mice showed a decrease in the number TRAP-positive OCs. Monocytes were isolated from the bone marrow and were induced to differentiate by M-CSF and RANKL. The cell cultures were stained for TRAP 5 days later. Bottom panel: quantitation data. Scale bar, 100 μm. N = 4 independent experiments.

(legend continued on next page)

of the nuclear factor κB (NF-κB) pathway (Figure 7F). This is consistent with previous reports showing that mTOR activation downregulated NF-κB signaling (Ghosh et al., 2006; Weichhart et al., 2008), the master regulator of OC differentiation, fusion, and activity.

We also isolated bone marrow monocytes from *Ctsk-Tsc1*$^{f/f}$ mice and performed ex vivo differentiation assays. These cells only express Cre after differentiating into Ctsk-positive OCs, which would then lead to *Tsc1* deletion. We found that the number and size of TRAP-positive OCs were slightly increased in the mutant cultures (Figure 7G). However, differentiated OCs derived from *Ctsk-Cre; Tsc1*$^{f/f}$ mice showed a decrease in bone resorption activity (Figure 7H). These results suggest that mTOR activation may promote proliferation and/or growth of differentiated osteoclasts, but interfere with their bone resorption activity. This may explain why *Ctsk-Cre; Tsc1*$^{f/f}$ mice showed an increase in the number of OCs.

We also investigated the mechanisms underlying the bone resorption defects caused by *Tsc1* deficiency. Although autophagy has been reported to play a role in bone resorption (Chagin, 2016; DeSelm et al., 2011), we found that in OC cultures, autophagy markers p62 and LC3 were not significantly altered in the absence of Tsc1 (Figure S7C). However, OCs showed an increase in size on bone sections of *Ctsk-Cre; Tsc1*$^{f/f}$ mice but not of *LysM-Cre; Tsc1*$^{f/f}$ mice (Figure S7D). Moreover, the number of ring-like actin structures was decreased in both mouse lines, with the decrease in *Ctsk-Cre; Tsc1*$^{f/f}$ mouse bone sections being greater than that in *LysM-Cre; Tsc1*$^{f/f}$ mice (Figure S7E). These alterations may contribute to the resorption defects of *Tsc1*-deficient OCs and explain why *Ctsk-Cre; Tsc1*$^{f/f}$ mice showed a greater osteopetrotic phenotype than *LysM-Cre; Tsc1*$^{f/f}$.

TSC Patients Showed Increased Focal Bone Density Accompanied by Increased Bone Formation and Decreased Bone Resorption

The above model animal studies indicate that mTOR signaling regulates bone size and quality during adolescent growth. We then wanted to validate these findings using TSC patient samples. TSC patients usually carry mutations in one allele of *TSC1* or *TSC2*, and loss of heterozygosity leads to benign tumor formation. We collected 64 TSC patients, 96.9% (62/64) of whom showed multiple sclerotic bone lesions in the vertebral body and appendix, the sternum, the rib, or the pelvis, on CT images (Figure 7I). We also collected serum samples from TSC patients between the ages 15 and 24 years to analyze bone formation marker osteocalcin and bone resorption marker CTX, and found that, compared with the age-matched normal group, TSC patients showed an increase in osteocalcin and a decrease in CTX (Figures 7J and 7K), suggesting that bone formation is increased while bone resorption is decreased in TSC patients.

DISCUSSION

This study, by analyzing mouse models with mTOR activated in BM-MSCs, monocytes, or their progenies, demonstrates that mTOR signaling regulates adolescent bone growth in size, mass, and mineral contents by acting on different cell types. mTOR activation in chondrocytes and OBs appears to be strong during adolescent growth and declines when reaching adulthood. mTOR activation increases bone radial growth, trabecular bone volume, and cortical bone thickness, mainly by promoting proliferation of *Prx1*+ BM-MSCs and increasing the pools of MSCs. However, mTOR activation decreases the length of long bones

(C) Images of WT and *Tsc1*$^{-/-}$ OCs. Scale bar, 50 μm.
(D) qPCR analysis revealed that *Tsc1* ablation in *LysM*+ monocytes showed a decrease in the expression of OC differentiation markers and genes regulating OC fusion. N = 4 independent experiments.
(E) *Tsc1*-deficient monocytes showed a decrease in bone resorption activity in vitro. Monocytes isolated from the *LysM-Cre; Tsc1*$^{f/f}$ mice were induced to differentiate by M-CSF and RANKL, and then plated onto dentine slices. After 5 days, the slices were stained with toluidine blue and the resorption areas were measured (bottom panel). Red arrow, resorption pit. N = 3 independent experiments.
(F) *Tsc1*$^{-/-}$ monocytes showed a decrease in NF-κB activation during OC differentiation.
(G) Ex vivo differentiation assays revealed that monocytes isolated from *Ctsk-Cre; Tsc1*$^{f/f}$ mice showed a slight increase in TRAP-positive OCs. Monocytes were isolated from the bone marrow and were induced to differentiate by M-CSF and RANKL. The cell cultures were stained for TRAP 5 days later. Bottom panel: quantitation data. Scale bar, 100 μm. N = 5 independent experiments.
(H) *Tsc1*-deficient OCs showed a decrease in bone resorption activity in vitro. Monocytes isolated from the *Ctsk-Cre; Tsc1*$^{f/f}$ mice were induced to differentiate by M-CSF and RANKL for 3 days, and then plated onto dentine slices. After 5 days, the slices were stained with toluidine blue and the resorption areas were measured (bottom panel). Red arrow, resorption pit. Scale bar, 50 μm. N = 3 independent experiments.
(I) CT images of TSC patients revealed sclerotic bone lesions (orange arrows) with roundish or irregular shape in the vertebral body and appendix of the cervical (a), thoracic (b), and lumbar (c) spine, as well as the sternum (d), rib (e), and pelvis (f).
(J) The TSC patient serum samples showed an increase in the levels of osteocalcin. N = 20.
(K) The TSC patient serum samples showed a decrease in the levels of CTX. N = 20.
Error bars represent the SD. *p < 0.05; **p < 0.01.

and bone mineralization, likely caused by impeded MSC chondrogenic and osteogenic differentiation, respectively (Figure S7F). These findings suggest that mTOR signaling coordinates MSC proliferation and differentiation to regulate bone size and quality, and that expansion of the BM-MSC pool is an important step during bone growth. The mTOR signaling pathway may integrate the signals from growth factors, nutrients, and other pathways such as Pten or LKB1 to regulate bone growth in length (Ford-Hutchinson et al., 2007; Lai et al., 2013; Shima et al., 1998).

mTOR activation in MSCs appears to impede bone mineralization, indicating that mTOR activation does not mediate the anabolic effects of growth factors on bone mineral accretion. Instead, mTOR activation suppresses the catabolic effects of monocyte/OC in cell-autonomous manners. While several in vitro studies suggest that inhibition of mTOR with rapamycin impedes OC survival and differentiation (Sugatani and Hruska, 2005), our study provides genetic evidence that mTOR activation inhibits OC differentiation, fusion, and resorption activity, but promotes proliferation of monocytes and differentiated OCs, suggesting stage-specific effects for mTOR in osteoclastogenesis and function (Figure S7F). OC differentiation and fusion defects may be caused by compromised NF-κB activation and decreased expression of cell fusion gene *DC-Stamp* and *OC-Stamp* (Figure S7F), while OC resorption defects may be caused by mTOR-induced alteration in cell size and/or cytoskeleton. The more severe osteopetrotic phenotype of *Ctsk-Cre; Tsc1*$^{f/f}$ than *LysM-Cre; Tsc1*$^{f/f}$ mice can be explained by the difference in OC cell size and cytoskeleton (Figures S7D and S7E). The lack of increase in OC numbers in *LysM-Cre; Tsc1*$^{f/f}$ mice could be caused by opposite and stage-specific effects of mTOR activation on OC proliferation and differentiation. It is worth noting that the peak bone mass is a net result of 10 weeks of bone formation and resorption, which may not be reflected by the bone parameters measured at week 10 of age or in vitro assays.

In addition, mTOR activation in MSCs, but not in OBs, plays a role in coupling to osteoclastogenesis. mTOR signaling in *Prx1*+ MSCs alters the expression of M-CSF, OPG, and RANKL to inhibit osteoclastogenesis and bone resorption. Consistently, previous studies of mouse lines with *Tsc1* ablated in Osx- or osteocalcin-expressing OBs failed to detect significant alterations in bone resorption (Chen and Long, 2014; Fang et al., 2015; Riddle et al., 2014). These findings support the concept that coupling exists between MSCs and monocytes in addition to the coupling between bone formation and resorption (Cong et al., 2016). Thus, mTOR increases bone mineral contents by directly inhibiting OC differentiation and activity, and by altering MSCs-secreted RANKL and OPG.

Our studies reveal that more than 90% TSC patients of Han Chinese develop focal sclerotic bone lesions at different locations in the skeleton. Analysis of TSC patient serum samples confirmed that bone resorption marker is reduced, whereas bone formation marker is increased. While it is assumed that increased focal bone density is secondary to increased bone formation (Umeoka et al., 2008), we found that, in mouse models, deletion of *Tsc1* in BM-MSCs or OBs led to a decrease in bone mineral contents. In contrast, deletion of *Tsc1* in monocytes especially in OCs led to a great increase in bone mineral contents. These data suggest that the increase in focal bone density in TSC patients is caused mainly by decreased bone resorption. Thus, sclerotic bone lesions should be deemed as "osteopetrotic lesions" in TSC patients.

Model animal and human sample studies have shown that hormone deficiency and undernutrition are the major factors affecting organ size, and which inhibit cell proliferation and cell size in the organ. Our current studies, together with the studies of OB- and chondrocyte-specific deletion of mTOR pathway molecules, indicate that mTOR signaling is an important regulator of bone size and quality. mTOR regulates bone size by acting on MSCs rather than OBs; its pro-proliferation activity in MSCs accounts for the bone radial growth and bone volume accrual, whereas its negative effects on MSC chondrogenic differentiation regulate bone growth in length. Therefore the coordination of MSC proliferation and differentiation controls bone growth in length and width.

In summary, we show that mTOR signaling regulates bone size mainly by coordinating MSC proliferation and differentiation, and bone quality mainly by suppressing OC differentiation and activity. Moreover, mTOR also plays a role in coupling MSCs and monocytes. Studies of TSC patient samples validated these findings. Collectively, our studies uncover multiple roles played by mTOR signaling in bone size and quality control.

EXPERIMENTAL PROCEDURES

TSC Patients

All the 64 TSC patients (38 women and 26 men; age range, 4–46 years; mean ± SD age, 26.1 ± 8.7 years) underwent CT examinations of the chest, abdomen, and pelvis using a SOMATOM Definition Flash scanner (Siemens Medical Systems) and a Discovery CT750 HD scanner (GE Medical Systems) with slice thickness of 5 mm and tube voltage of 120 kvp. The protocol for this study was approved by our institutional review board. All patients gave written consent.

Animal Studies

Animal work was carried out following the recommendations from the National Research Council Guide for the Care and Use of Laboratory Animals, with the protocols approved by the Institutional Animal Care and Use Committee of Shanghai, China (SYXK(SH)

2011-0112). The *Prx1-Cre*, *Dermo1-Cre*, *Osx-Cre*, *LysM-Cre*, *Ctsk-Cre*, and floxed *Tsc1* mouse lines were purchased from The Jackson Laboratory. For micro-CT and histomorphometry analysis, male mice at age 2.5 months were used, with the number of mice shown for each figure. For other mouse experiments, three mice (2.5-month-old male or female) were used.

Bone Histomorphometry and Three-Point Bending Experiment

Bone histomorphometry was performed on undecalcified sections as described in the Supplemental Information, and three-point bending experiments were conducted on a universal testing machine (RGM-2020, Shenzhen Reger Instrument) using fixed femurs.

Measurement of Serum Osteocalcin and CTX and Urine DPD

Fasting serum samples of TSC patients and normal individuals were collected to determine the levels of osteocalcin and CTX. Mouse urine samples were collected in the morning and were used to determine the levels of DPD and creatinine. The DPD values were normalized to creatinine.

BM-MSC Isolation and Differentiation

BM-MSCs were isolated and induced to differentiate as described by Cong et al. (2016).

Monocyte Isolation and Differentiation and Resorption Pit Analysis

BM-MSCs were isolated and induced to differentiate as described by Cong et al. (2016).

qPCR

Total RNA was extracted by using TRIzol Regent (Invitrogen). The RNA was reverse transcribed using a Transcriptor Universal cDNA Master (Roche) according to the manufacturer's instructions. Real-time PCR was performed as described previously (Cong et al., 2016). See Supplemental Information for primer sequences.

Immunohistochemical Staining

See Supplemental Information for detailed protocols.

Statistical Analyses

Numerical data and histograms were expressed as the mean ± SD. Comparisons between two groups were analyzed using two-tailed unpaired Student's t test. p Values < 0.05 were considered statistically significant. Analysis of mice was litter-based, and at least three litters were analyzed for every parameter. All experiments were repeated three to four times.

SUPPLEMENTAL INFORMATION

Supplemental Information includes Supplemental Experimental Procedures and seven figures and can be found with this article online at http://dx.doi.org/10.1016/j.stemcr.2017.04.005.

AUTHOR CONTRIBUTIONS

B.L., H.Z., Z.Z., and W.Z. designed the research. H.W., Z.W., P.L., Q.C., R.C., W.X., S.W., H.L., X.X., S.L., W.H., L.Z., J.Z., and S.L.H. performed the research. H.W., Z.W., and W.Z. analyzed the data; W.X., H.Z., W.H., and Z.Z. provided the TSC patient samples. H.L. and B.L. wrote the paper.

ACKNOWLEDGMENT

The work was supported by the National Key Scientific Program (2014CB942902 and 2012CB966901) and the National Natural Science Foundation of China (81520108012 and 91542120).

Received: June 18, 2016
Revised: April 5, 2017
Accepted: April 5, 2017
Published: May 4, 2017

REFERENCES

Avila, N.A., Dwyer, A.J., Rabel, A., Darling, T., Hong, C.H., and Moss, J. (2010). CT of sclerotic bone lesions: imaging features differentiating tuberous sclerosis complex with lymphangioleiomyomatosis from sporadic lymphangioleiomymatosis. Radiology *254*, 851–857.

Baxter-Jones, A.D., Faulkner, R.A., Forwood, M.R., Mirwald, R.L., and Bailey, D.A. (2011). Bone mineral accrual from 8 to 30 years of age: an estimation of peak bone mass. J. Bone Miner. Res. *26*, 1729–1739.

Bonjour, J.P., and Chevalley, T. (2014). Pubertal timing, bone acquisition, and risk of fracture throughout life. Endocr. Rev. *35*, 820–847.

Callewaert, F., Venken, K., Kopchick, J.J., Torcasio, A., van Lenthe, G.H., Boonen, S., and Vanderschueren, D. (2010). Sexual dimorphism in cortical bone size and strength but not density is determined by independent and time-specific actions of sex steroids and IGF-1: evidence from pubertal mouse models. J. Bone Miner. Res. *25*, 617–626.

Canalis, E. (2009). Growth factor control of bone mass. J. Cell. Biochem. *108*, 769–777.

Chagin, A.S. (2016). Effectors of mTOR-autophagy pathway: targeting cancer, affecting the skeleton. Curr. Opin. Pharmacol. *28*, 1–7.

Chen, J., and Long, F. (2014). mTORC1 signaling controls mammalian skeletal growth through stimulation of protein synthesis. Development *141*, 2848–2854.

Clausen, B.E., Burkhardt, C., Reith, W., Renkawitz, R., and Forster, I. (1999). Conditional gene targeting in macrophages and granulocytes using LysMcre mice. Transgenic Res. *8*, 265–277.

Cong, Q., Jia, H., Biswas, S., Li, P., Qiu, S., Deng, Q., Guo, X., Ma, G., Ling Chau, J.F., Wang, Y., et al. (2016). p38alpha MAPK regulates lineage commitment and OPG synthesis of bone marrow stromal cells to prevent bone loss under physiological and pathological conditions. Stem Cell Rep. *6*, 566–578.

Csibi, A., and Blenis, J. (2012). Hippo-YAP and mTOR pathways collaborate to regulate organ size. Nat. Cell Biol. *14*, 1244–1245.

DeSelm, C.J., Miller, B.C., Zou, W., Beatty, W.L., van Meel, E., Takahata, Y., Klumperman, J., Tooze, S.A., Teitelbaum, S.L., and Virgin, H.W. (2011). Autophagy proteins regulate the secretory component of OCic bone resorption. Dev. Cell *21*, 966–974.

Edwards, J.R., and Mundy, G.R. (2011). Advances in OC biology: old findings and new insights from mouse models. Nat. Rev. Rheumatol. *7*, 235–243.

Fang, F., Sun, S., Wang, L., Guan, J.L., Giovannini, M., Zhu, Y., and Liu, F. (2015). Neural crest-specific TSC1 deletion in mice leads to sclerotic craniofacial bone lesion. J. Bone Miner. Res. *30*, 1195–1205.

Farr, J.N., and Khosla, S. (2015). Skeletal changes through the lifespan – from growth to senescence. Nat. Rev. Endocrinol. *11*, 513–521.

Ford-Hutchinson, A.F., Ali, Z., Lines, S.E., Hallgrimsson, B., Boyd, S.K., and Jirik, F.R. (2007). Inactivation of Pten in osteo-chondroprogenitor cells leads to epiphyseal growth plate abnormalities and skeletal overgrowth. J. Bone Miner. Res. *22*, 1245–1259.

Gao, B., Song, H., Bishop, K., Elliot, G., Garrett, L., English, M.A., Andre, P., Robinson, J., Sood, R., Minami, Y., et al. (2011). Wnt signaling gradients establish planar cell polarity by inducing Vangl2 phosphorylation through Ror2. Dev. Cell *20*, 163–176.

Ghosh, S., Tergaonkar, V., Rothlin, C.V., Correa, R.G., Bottero, V., Bist, P., Verma, I.M., and Hunter, T. (2006). Essential role of tuberous sclerosis genes TSC1 and TSC2 in NF-kappaB activation and cell survival. Cancer Cell *10*, 215–226.

Harada, S., and Rodan, G.A. (2003). Control of OB function and regulation of bone mass. Nature *423*, 349–355.

Hay, N., and Sonenberg, N. (2004). Upstream and downstream of mTOR. Genes Dev. *18*, 1926–1945.

Helming, L., and Gordon, S. (2009). Molecular mediators of macrophage fusion. Trends Cell Biol. *19*, 514–522.

Hendrickx, G., Boudin, E., and Van Hul, W. (2015). A look behind the scenes: the risk and pathogenesis of primary osteoporosis. Nat. Rev. Rheumatol. *11*, 462–474.

Henriksen, K., Karsdal, M.A., and Martin, T.J. (2014). OC-derived coupling factors in bone remodeling. Calcif. Tissue Int. *94*, 88–97.

Huang, B., Wang, Y., Wang, W., Chen, J., Lai, P., Liu, Z., Yan, B., Xu, S., Zhang, Z., Zeng, C., et al. (2015). mTORC1 prevents PreOB differentiation through the Notch signaling pathway. PLoS Genet. *11*, 1005426.

Huegel, J., Mundy, C., Sgariglia, F., Nygren, P., Billings, P.C., Yamaguchi, Y., Koyama, E., and Pacifici, M. (2013). Perichondrium phenotype and border function are regulated by Ext1 and heparan sulfate in developing long bones: a mechanism likely deranged in Hereditary Multiple Exostoses. Dev. Biol. *377*, 100–112.

Jewell, J.L., Russell, R.C., and Guan, K.L. (2013). Amino acid signalling upstream of mTOR. Nat. Rev. Mol. Cell Biol. *14*, 133–139.

Johnson, S.C., Rabinovitch, P.S., and Kaeberlein, M. (2013). mTOR is a key modulator of ageing and age-related disease. Nature *493*, 338–345.

Jones, K.B., Piombo, V., Searby, C., Kurriger, G., Yang, B., Grabellus, F., Roughley, P.J., Morcuende, J.A., Buckwalter, J.A., Capecchi, M.R., et al. (2010). A mouse model of osteochondromagenesis from clonal inactivation of Ext1 in chondrocytes. Proc. Natl. Acad. Sci. USA *107*, 2054–2059.

Karsenty, G., Kronenberg, H.M., and Settembre, C. (2009). Genetic control of bone formation. Annu. Rev. Cell Dev. Biol. *25*, 629–648.

Kronenberg, H.M. (2006). PTHrP and skeletal development. Ann. N. Y. Acad. Sci. *1068*, 1–13.

Lacey, D.L., Boyle, W.J., Simonet, W.S., Kostenuik, P.J., Dougall, W.C., Sullivan, J.K., San Martin, J., and Dansey, R. (2012). Bench to bedside: elucidation of the OPG-RANK-RANKL pathway and the development of denosumab. Nat. Rev. Drug Discov. *11*, 401–419.

Lai, L.P., Lilley, B.N., Sanes, J.R., and McMahon, A.P. (2013). Lkb1/Stk11 regulation of mTOR signaling controls the transition of chondrocyte fates and suppresses skeletal tumor formation. Proc. Natl. Acad. Sci. USA *110*, 19450–19455.

Laplante, M., and Sabatini, D.M. (2012). mTOR signaling in growth control and disease. Cell *149*, 274–293.

Lee, K., Deeds, J.D., and Segre, G.V. (1995). Expression of parathyroid hormone-related peptide and its receptor messenger ribonucleic acids during fetal development of rats. Endocrinology *136*, 453–463.

Li, P., Boronat, S., Geffrey, A.L., Barber, I., Grottkau, B.E., and Thiele, E.A. (2015). Rib and vertebral bone fibrous dysplasia in a child with tuberous sclerosis complex. Am. J. Med. Genet. A *167A*, 2755–2757.

Logan, M., Martin, J.F., Nagy, A., Lobe, C., Olson, E.N., and Tabin, C.J. (2002). Expression of Cre Recombinase in the developing mouse limb bud driven by a Prxl enhancer. Genesis *33*, 77–80.

Meikle, L., Talos, D.M., Onda, H., Pollizzi, K., Rotenberg, A., Sahin, M., Jensen, F.E., and Kwiatkowski, D.J. (2007). A mouse model of tuberous sclerosis: neuronal loss of Tsc1 causes dysplastic and ectopic neurons, reduced myelination, seizure activity, and limited survival. J. Neurosci. *27*, 5546–5558.

Penzo-Mendez, A.I., and Stanger, B.Z. (2015). Organ-size regulation in mammals. Cold Spring Harb. Perspect. Biol. *7*, a019240.

Rafal, R.B., Ndzengue, A., and Jaffe, E.A. (2013). Tuberous sclerosis: computed tomography diagnosis. J. Emerg. Med. *44*, 259–261.

Riddle, R.C., Frey, J.L., Tomlinson, R.E., Ferron, M., Li, Y., DiGirolamo, D.J., Faugere, M.C., Hussain, M.A., Karsenty, G., and Clemens, T.L. (2014). Tsc2 is a molecular checkpoint controlling OB development and glucose homeostasis. Mol. Cell. Biol. *34*, 1850–1862.

Rodda, S.J., and McMahon, A.P. (2006). Distinct roles for Hedgehog and canonical Wnt signaling in specification, differentiation and maintenance of OB progenitors. Development *133*, 3231–3244.

Rosello-Diez, A., and Joyner, A.L. (2015). Regulation of long bone growth in vertebrates; it is time to catch up. Endocr. Rev. *36*, 646–680.

Shima, H., Pende, M., Chen, Y., Fumagalli, S., Thomas, G., and Kozma, S.C. (1998). Disruption of the p70(s6k)/p85(s6k) gene reveals a small mouse phenotype and a new functional S6 kinase. EMBO. J. *17*, 6649–6659.

Sugatani, T., and Hruska, K.A. (2005). Akt1/Akt2 and mammalian target of rapamycin/Bim play critical roles in OC differentiation

and survival, respectively, whereas Akt is dispensable for cell survival in isolated OC precursors. J. Biol. Chem. *280*, 3583–3589.

Umeoka, S., Koyama, T., Miki, Y., Akai, M., Tsutsui, K., and Togashi, K. (2008). Pictorial review of tuberous sclerosis in various organs. Radiographics *28*, 32.

Wang, Q., Ghasem-Zadeh, A., Wang, X.F., Iuliano-Burns, S., and Seeman, E. (2011). Trabecular bone of growth plate origin influences both trabecular and cortical morphology in adulthood. J. Bone Miner. Res. *26*, 1577–1583.

Weichhart, T., Costantino, G., Poglitsch, M., Rosner, M., Zeyda, M., Stuhlmeier, K.M., Kolbe, T., Stulnig, T.M., Horl, W.H., Hengstschlager, M., et al. (2008). The TSC-mTOR signaling pathway regulates the innate inflammatory response. Immunity *29*, 565–577.

Whiting, S.J., Vatanparast, H., Baxter-Jones, A., Faulkner, R.A., Mirwald, R., and Bailey, D.A. (2004). Factors that affect bone mineral accrual in the adolescent growth spurt. J. Nutr. *134*, 696S–700S.

Yakar, S., Courtland, H.W., and Clemmons, D. (2010). IGF-1 and bone: new discoveries from mouse models. J. Bone Miner. Res. *25*, 2543–2552.

Yan, B., Zhang, Z., Jin, D., Cai, C., Jia, C., Liu, W., Wang, T., Li, S., Zhang, H., Huang, B., et al. (2016). mTORC1 regulates PTHrP to coordinate chondrocyte growth, proliferation and differentiation. Nat. Commun. *7*, 11151.

Yang, Y., Topol, L., Lee, H., and Wu, J. (2003). Wnt5a and Wnt5b exhibit distinct activities in coordinating chondrocyte proliferation and differentiation. Development *130*, 1003–1015.

Yu, K., Xu, J., Liu, Z., Sosic, D., Shao, J., Olson, E.N., Towler, D.A., and Ornitz, D.M. (2003). Conditional inactivation of FGF receptor 2 reveals an essential role for FGF signaling in the regulation of OB function and bone growth. Development *130*, 3063–3074.

Zemel, B. (2013). Bone mineral accretion and its relationship to growth, sexual maturation and body composition during childhood and adolescence. World Rev. Nutr. Diet. *106*, 39–45.

Stem Cell Reports, Volume *8*

Supplemental Information

Bone Size and Quality Regulation: Concerted Actions of mTOR in Mesenchymal Stromal Cells and Osteoclasts

Hongguang Wu, Zhixiang Wu, Ping Li, Qian Cong, Rongrong Chen, Wenrui Xu, Soma Biswas, Huijuan Liu, Xuechun Xia, Shanshan Li, Weiwei Hu, Zhenlin Zhang, Samy L. Habib, Lingli Zhang, Jun Zou, Hongbing Zhang, Weihong Zhang, and Baojie Li

Figure S1

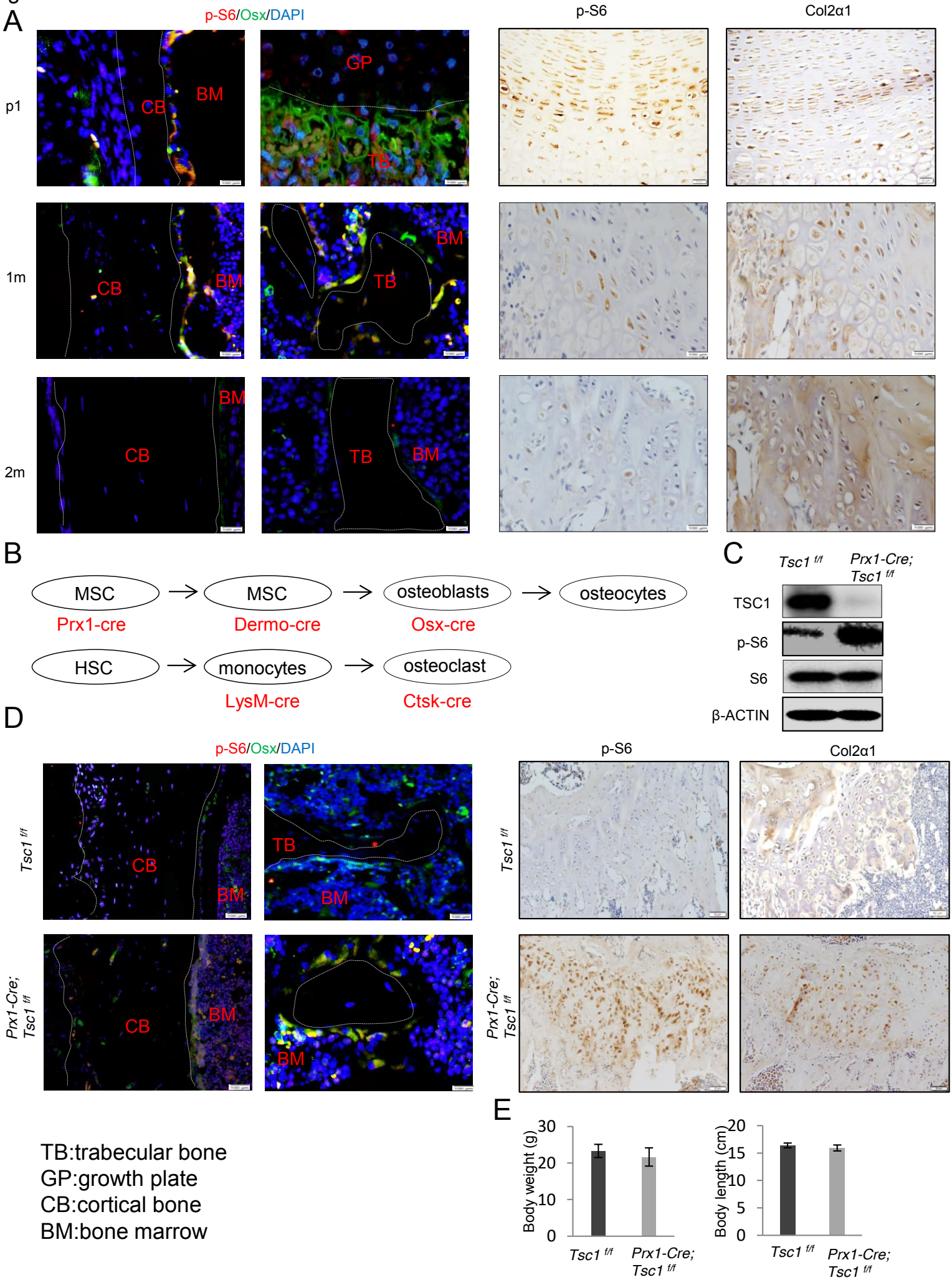

TB:trabecular bone
GP:growth plate
CB:cortical bone
BM:bone marrow

Figure S2

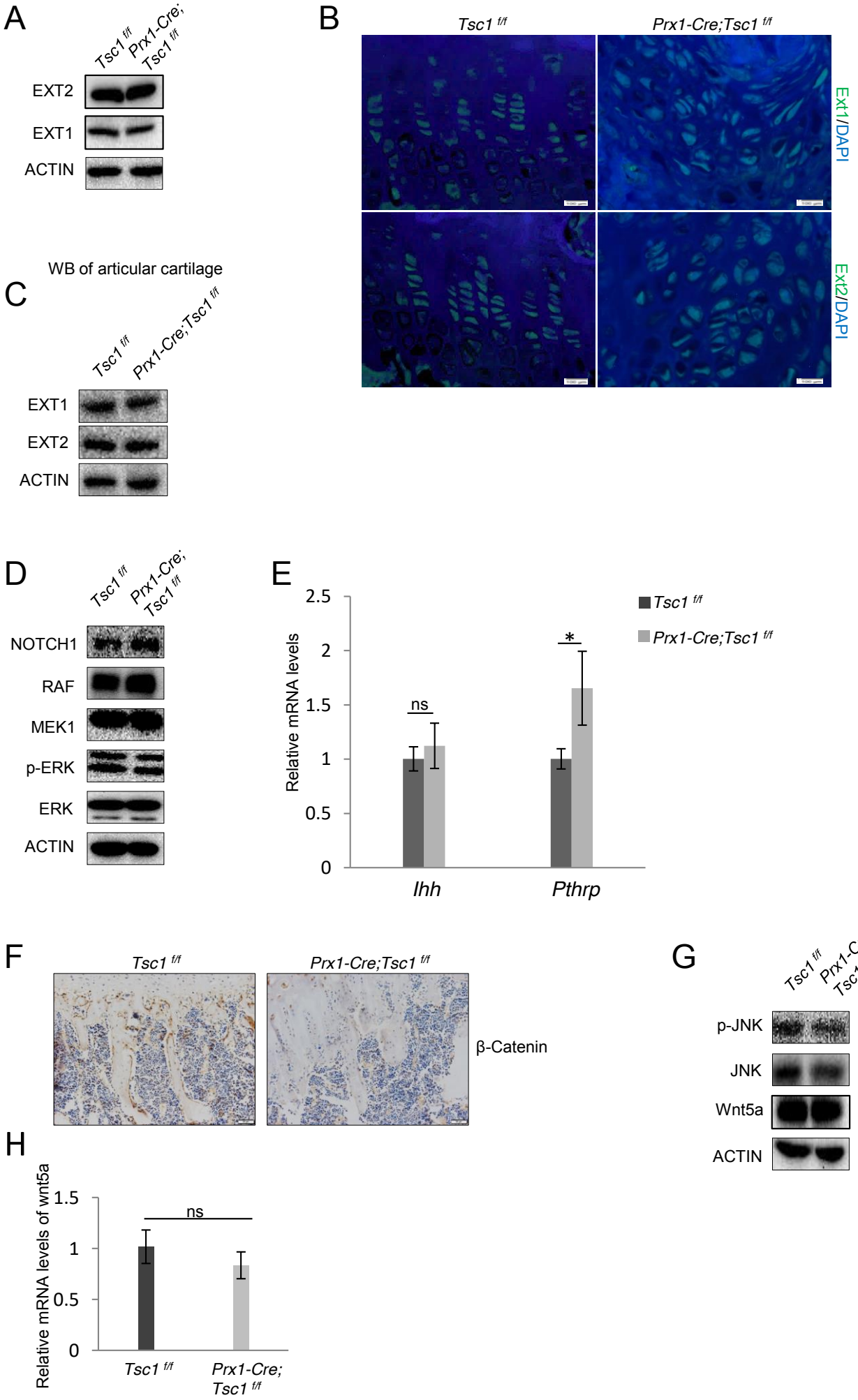
A
Tsc1 f/f
Prx1-Cre; Tsc1 f/f
EXT2
EXT1
ACTIN
B
Tsc1 f/f
Prx1-Cre;Tsc1 f/f
Ext1/DAPI
Ext2/DAPI
WB of articular cartilage
C
Tsc1 f/f
Prx1-Cre;Tsc1 f/f
EXT1
EXT2
ACTIN
D
Tsc1 f/f
Prx1-Cre; Tsc1 f/f
NOTCH1
RAF
MEK1
p-ERK
ERK
ACTIN
E
Tsc1 f/f
Prx1-Cre;Tsc1 f/f
Relative mRNA levels
2.5
2
1.5
1
0.5
0
ns
*
Ihh
Pthrp
F
Tsc1 f/f
Prx1-Cre;Tsc1 f/f
β-Catenin
G
Tsc1 f/f
Prx1-Cre; Tsc1 f/f
p-JNK
JNK
Wnt5a
ACTIN
H
Relative mRNA levels of wnt5a
1.5
1
0.5
0
ns
Tsc1 f/f
Prx1-Cre; Tsc1 f/f

Figure S3

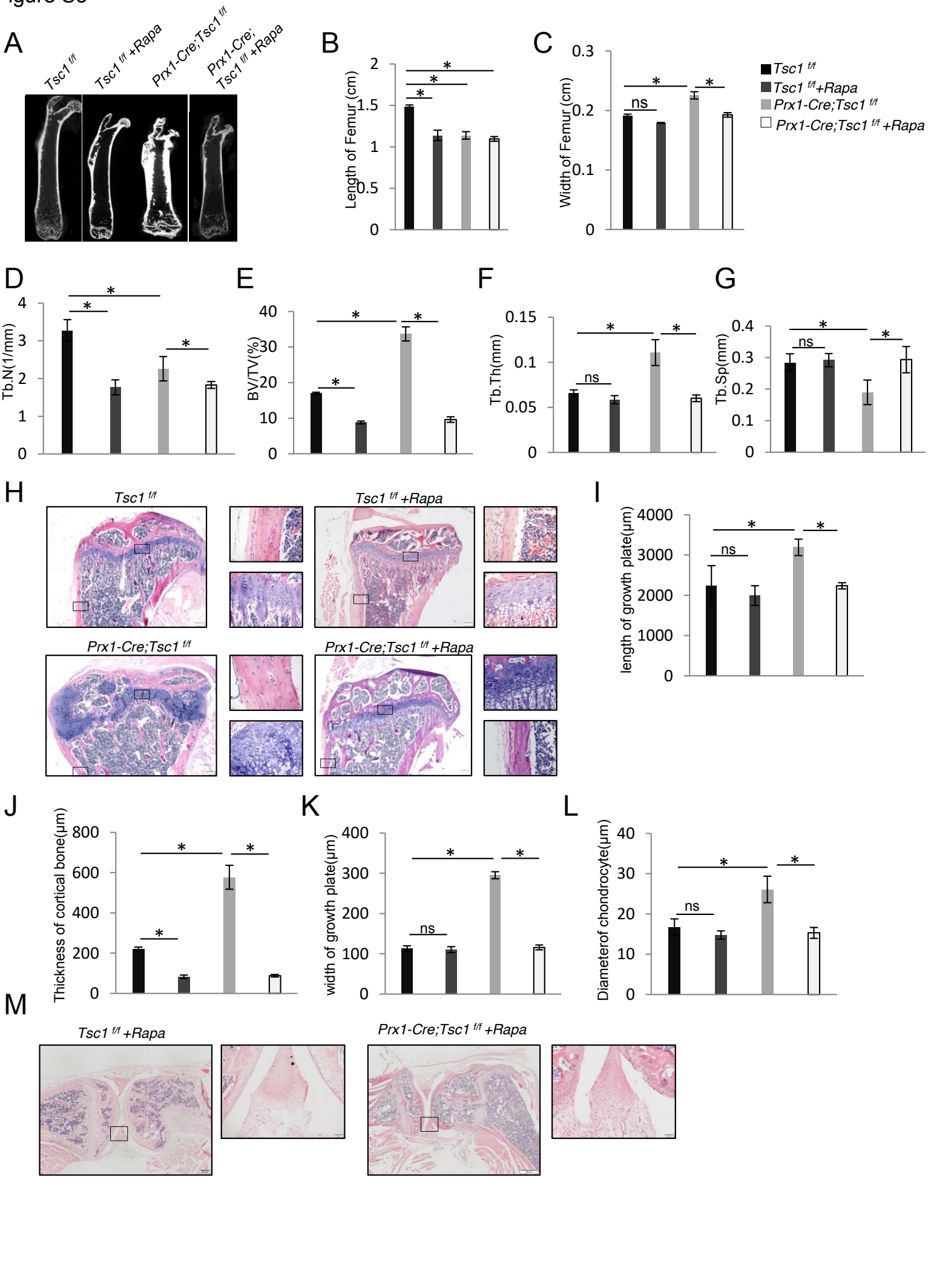
A
Tsc1 f/f
Tsc1 f/f +Rapa
Prx1-Cre;Tsc1 f/f
Prx1-Cre; Tsc1 f/f +Rapa
B
Length of Femur (cm)
C
Width of Femur (cm)
ns
Tsc1 f/f
Tsc1 f/f+Rapa
Prx1-Cre;Tsc1 f/f
Prx1-Cre;Tsc1 f/f +Rapa
D
Tb.N(1/mm)
E
BV/TV(%)
F
Tb.Th(mm)
G
Tb.Sp(mm)
H
Tsc1 f/f
Tsc1 f/f +Rapa
Prx1-Cre;Tsc1 f/f
Prx1-Cre;Tsc1 f/f +Rapa
I
length of growth plate(μm)
J
Thickness of cortical bone(μm)
K
width of growth plate(μm)
L
Diameterof chondrocyte(μm)
M
Tsc1 f/f +Rapa
Prx1-Cre;Tsc1 f/f +Rapa

Figure S4

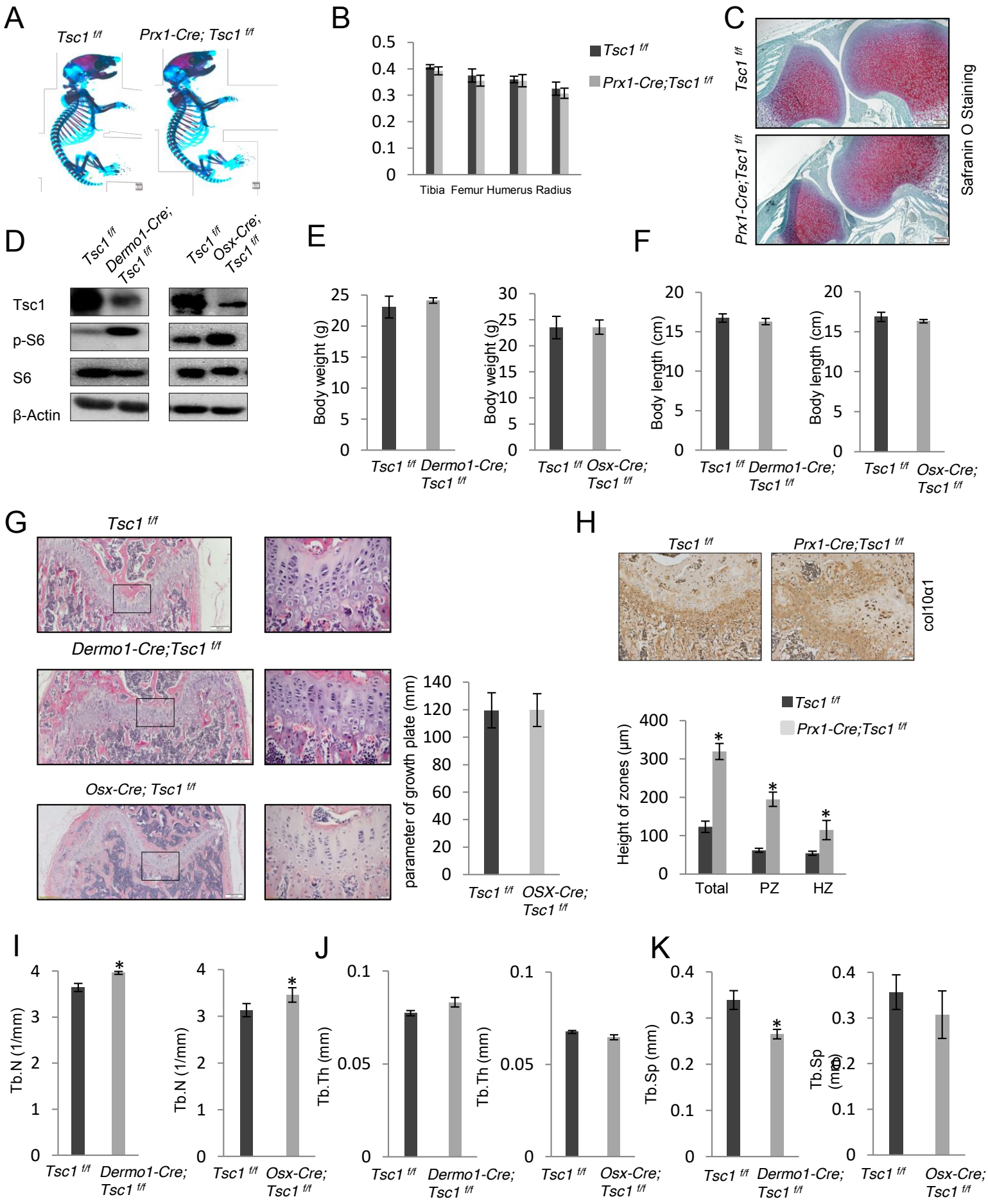
A
Tsc1 f/f
Prx1-Cre; Tsc1 f/f
B
Tsc1 f/f
Prx1-Cre;Tsc1 f/f
Tibia Femur Humerus Radius
C
Tsc1 f/f
Prx1-Cre;Tsc1 f/f
Safranin O Staining
D
Tsc1 f/f Dermo1-Cre; Tsc1 f/f
Tsc1 f/f Osx-Cre; Tsc1 f/f
Tsc1
p-S6
S6
β-Actin
E
Body weight (g)
Tsc1 f/f Dermo1-Cre; Tsc1 f/f
Tsc1 f/f Osx-Cre; Tsc1 f/f
F
Body length (cm)
Tsc1 f/f Dermo1-Cre; Tsc1 f/f
Tsc1 f/f Osx-Cre; Tsc1 f/f
G
Tsc1 f/f
Dermo1-Cre;Tsc1 f/f
Osx-Cre; Tsc1 f/f
parameter of growth plate (mm)
Tsc1 f/f OSX-Cre; Tsc1 f/f
H
Tsc1 f/f
Prx1-Cre;Tsc1 f/f
col10α1
Tsc1 f/f
Prx1-Cre;Tsc1 f/f
Height of zones (μm)
Total PZ HZ
I
Tb.N (1/mm)
Tsc1 f/f Dermo1-Cre; Tsc1 f/f
Tsc1 f/f Osx-Cre; Tsc1 f/f
J
Tb.Th (mm)
Tsc1 f/f Dermo1-Cre; Tsc1 f/f
Tsc1 f/f Osx-Cre; Tsc1 f/f
K
Tb.Sp (mm)
Tsc1 f/f Dermo1-Cre; Tsc1 f/f
Tsc1 f/f Osx-Cre; Tsc1 f/f

Figure S5

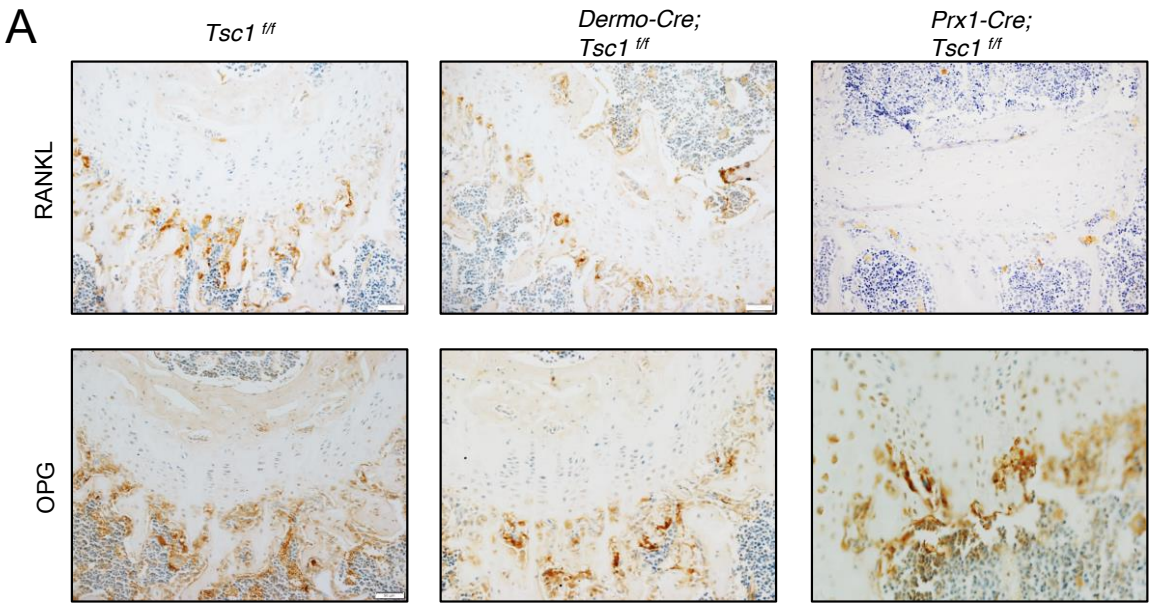
A
Tsc1 f/f
Dermo-Cre; Tsc1 f/f
Prx1-Cre; Tsc1 f/f
RANKL
OPG

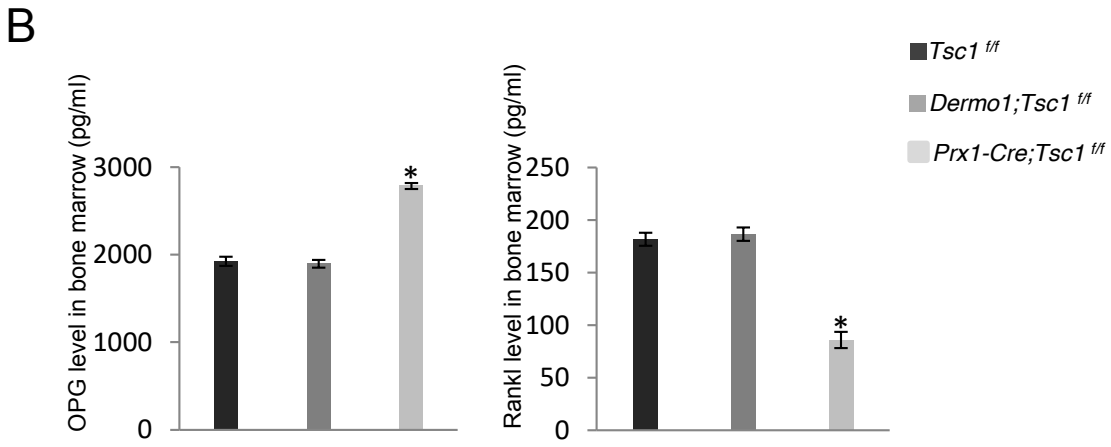
B
OPG level in bone marrow (pg/ml)
3000
2000
1000
0
*
Rankl level in bone marrow (pg/ml)
250
200
150
100
50
0
*
Tsc1 f/f
Dermo1;Tsc1 f/f
Prx1-Cre;Tsc1 f/f

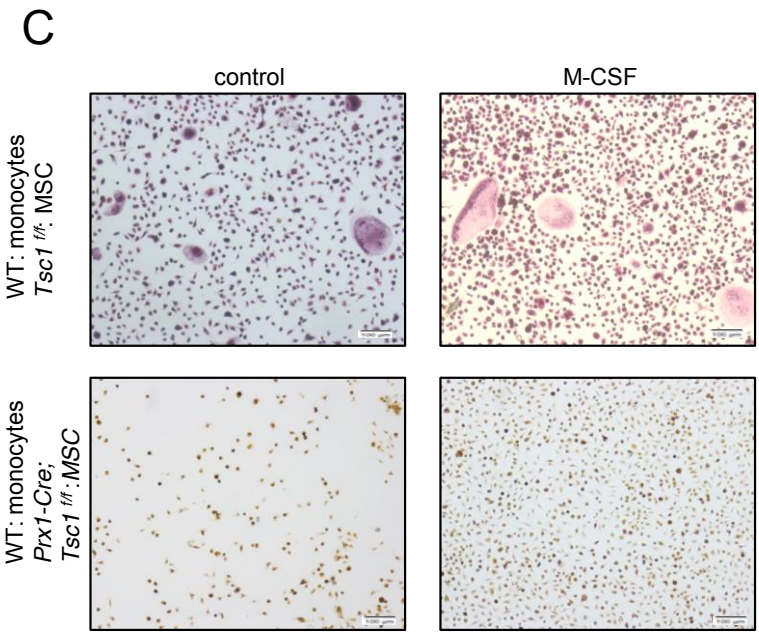
C
control
M-CSF
WT: monocytes
Tsc1 f/f: MSC
WT: monocytes
Prx1-Cre;
Tsc1 f/f :MSC

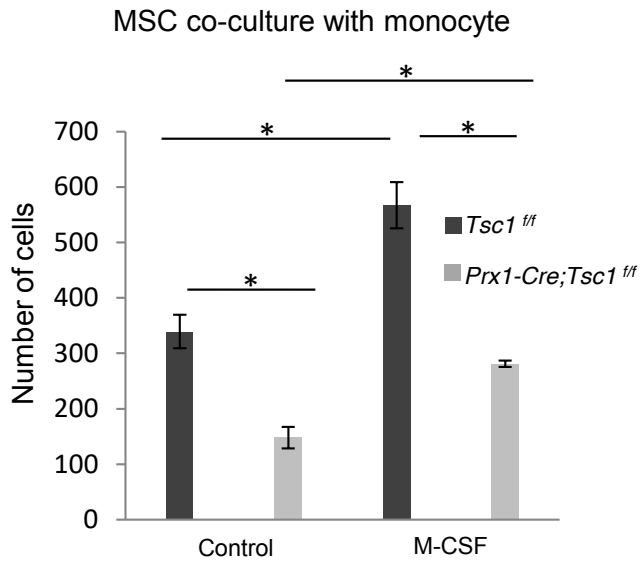
MSC co-culture with monocyte
Number of cells
700
600
500
400
300
200
100
0
*
*
*
*
Tsc1 f/f
Prx1-Cre;Tsc1 f/f
Control
M-CSF

Figure S6

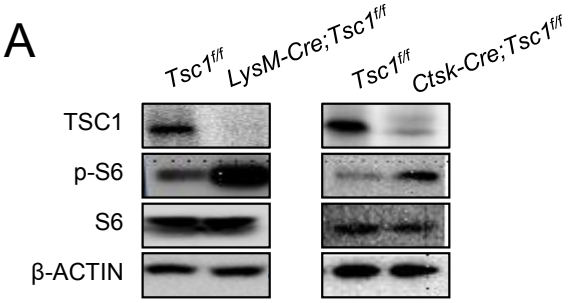
A
Tsc1f/f
LysM-Cre;Tsc1f/f
Tsc1f/f
Ctsk-Cre;Tsc1f/f
TSC1
p-S6
S6
β-ACTIN

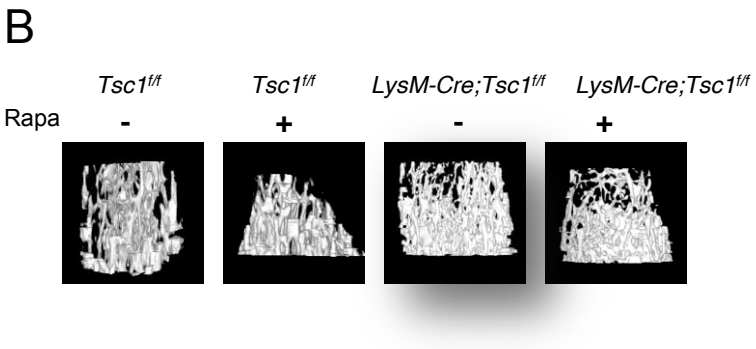
B
Tsc1f/f
Tsc1f/f
LysM-Cre;Tsc1f/f
LysM-Cre;Tsc1f/f
Rapa
-
+
-
+

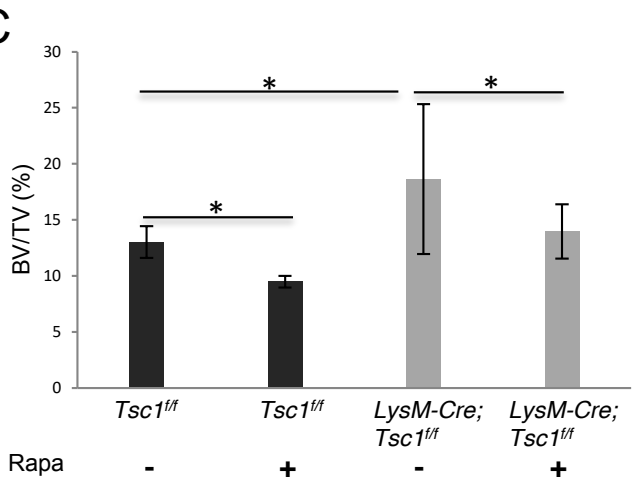
C
BV/TV (%)
30
25
20
15
10
5
0
*
*
*
Tsc1f/f
Tsc1f/f
LysM-Cre; Tsc1f/f
LysM-Cre; Tsc1f/f
Rapa
-
+
-
+

Figure S7

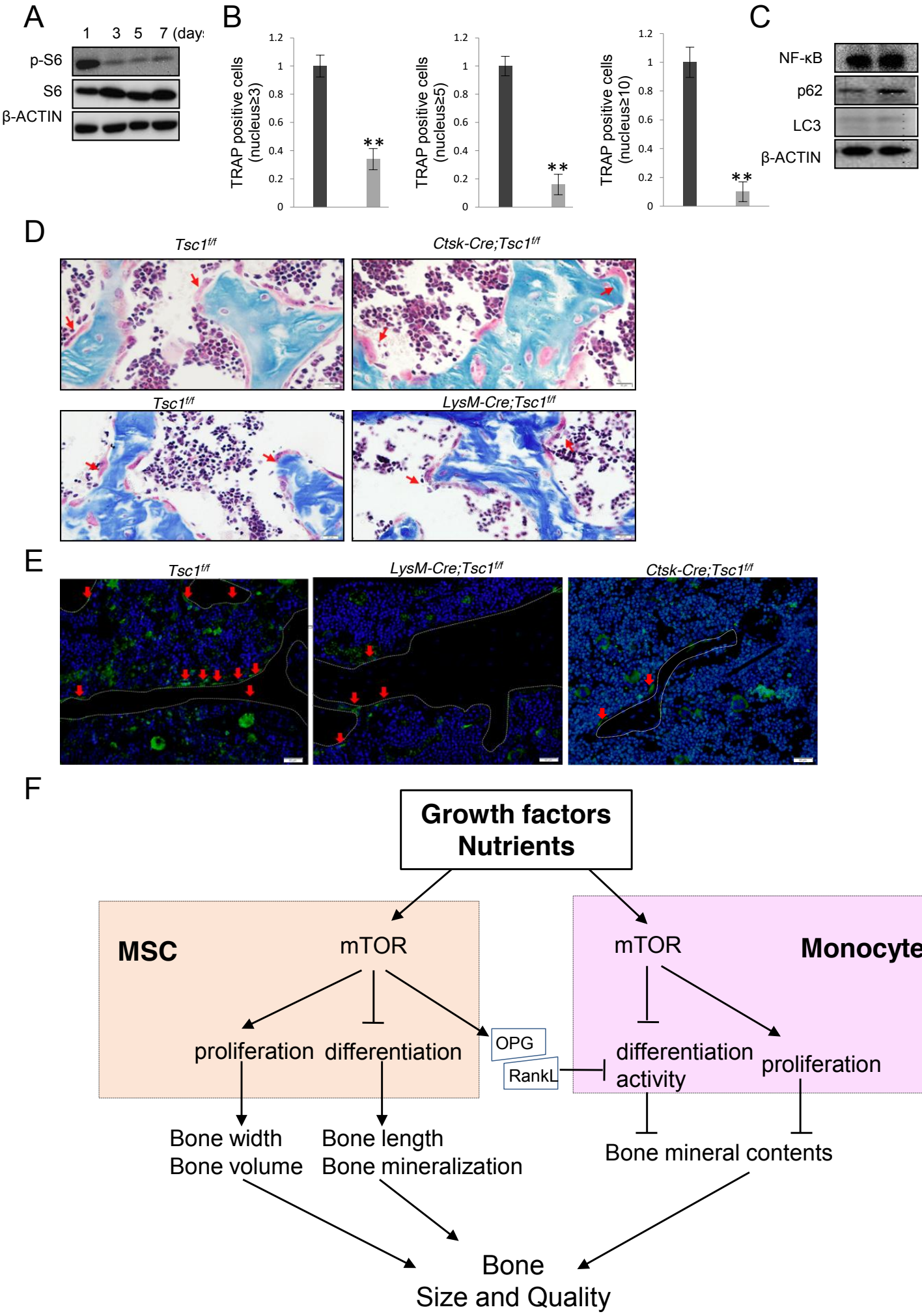
A
1 3 5 7 (day
p-S6
S6
β-ACTIN
B
TRAP positive cells (nucleus≥3)
TRAP positive cells (nucleus≥5)
TRAP positive cells (nucleus≥10)
**
C
NF-κB
p62
LC3
β-ACTIN
D
Tsc1f/f
Ctsk-Cre;Tsc1f/f
Tsc1f/f
LysM-Cre;Tsc1f/f
E
Tsc1f/f
LysM-Cre;Tsc1f/f
Ctsk-Cre;Tsc1f/f
F
Growth factors
Nutrients
MSC
mTOR
proliferation
differentiation
OPG
RankL
mTOR
Monocyte
differentiation activity
proliferation
Bone width
Bone volume
Bone length
Bone mineralization
Bone mineral contents
Bone
Size and Quality

Supplementary Figure legend

Figure S1. Staining of p-S6 and Osx or Col2α on bone sections of *WT* and *Prx1-Cre; Tsc1$^{f/f}$* mice, related to Figure 1.

A. Staining of p-S6 and Osx (left panels) or Col2α (right panels) on bone sections of p1, 1-month-old, and 2-month-old WT mice, showing mTOR activation at growth plate, trabecular bone, and periosteal/endosteal surfaces. Note that the anti-Col2α and p-S6 antibodies are from the same species so we stained them on separate sections. Scale bar, 50 μm.
B. A diagram to show the *Cre* mice that were used to ablate *Tsc1* in different cells along the lines of osteoblast and osteoclast differentiation.
C. Western blot showed that deletion of *Tsc1* led to mTOR activation in BM-MSCs, manifested an increase in p-S6. Scale bar, 50 μm.
D. Staining of p-S6 and Osx (left panels) or Col2α (right panels) on bone sections of *Prx1-Cre; Tsc1$^{f/f}$* and control mice, showing mTOR activation was enhanced in the mutant mice at growth plate, trabecular bone, and periosteal/endosteal surfaces. Scale bar, 50 μm.
E. Normal body weights and body lengths of *Prx1-Cre; Tsc1$^{f/f}$* compared to control male mice at 2.5 month of age. N=15 mice.

Figure S2. The expression and/or activation of mTOR-independent pathway molecules, β-Catenin-independent pathway molecules and Ext1/2, related to Figure 2 and 4.

A. Western blot results showed that the protein levels of EXT1 and EXT2 were unaltered in *Tsc1$^{-/-}$* BM-MSCs compared to control BM-MSCs.
B. Staining of EXT1 and EXT2 on femur bone sections of *Prx1-Cre; Tsc1$^{f/f}$* and WT mice. Scale bar, 50 μm.
C. Western blot results showed that the protein levels of EXT1 and EXT2 were unaltered in *Tsc1$^{-/-}$* femur head cartilage samples compared to control samples.
D. Western blot results showed that NOTCH1 protein levels were increased while

the levels of B-RAF, MEK1, or p-ERK2 were unaltered in *Tsc1*$^{-/-}$ BM-MSCs compared to control BM-MSCs.

E. Quantitative PCR showed that *Tsc1* deletion increased the mRNA levels of *Pthrp* but not *Ihh* in BM-MSCs. The experiments were repeated 3 times with triplicate.

F. Immuno-staining for β-Catenin on femur sections of *Prx1-Cre; Tsc1*$^{f/f}$ and control mice, showing that β-Catenin was decreased on *Prx1-Cre; Tsc1*$^{f/f}$ mouse bones. Scale bar, 50 μm.

G. Western blot results showed that *Tsc1* deletion decreased the activation of JNK without affecting the expression of WNT5a in BM-MSCs.

H. Quantitative PCR showed unaltered mRNA levels of *Wnt5a* in *Tsc1*$^{-/-}$ BM-MSCs compared to control BM-MSCs. The experiments were repeated 3 times with triplicate.

Figure S3. Rapamycin treatment largely rescued the histomorphometry indices and the growth plate and joint defects of *Prx1-Cre; Tsc1*$^{f/f}$ mice, related to Figure 2 and 3. Rapamycin was intraperitoneally injected into 3-week-old mutant and control mice at the dose of 3 μg/g body weight per day for 40 days. N=5 mice.

A. Micro-CT images of the femurs of rapamycin (rapa) or solvent-treated *Tsc1*$^{f/f}$ and *Prx1-Cre; Tsc1*$^{f/f}$ mice.

B. The femur length of rapamycin or solvent-treated *Tsc1*$^{f/f}$ and *Prx1-Cre; Tsc1*$^{f/f}$ mice.

C. The femur width of rapamycin or solvent-treated *Tsc1*$^{f/f}$ and *Prx1-Cre; Tsc1*$^{f/f}$ mice.

D. The number of trabecular bones of rapamycin or solvent-treated *Tsc1*$^{f/f}$ and *Prx1-Cre; Tsc1*$^{f/f}$ mice.

E. The BV/TV of rapamycin or solvent-treated *Tsc1*$^{f/f}$ and *Prx1-Cre; Tsc1*$^{f/f}$ mice.

F. The thickness of the trabecular bones of rapamycin or solvent-treated *Tsc1*$^{f/f}$ and *Prx1-Cre; Tsc1*$^{f/f}$ mice.

G. The separation of trabecular bones of rapamycin or solvent-treated *Tsc1*$^{f/f}$ and

Prx1-Cre; Tsc1$^{f/f}$ mice.

H. H/E staining of the decalcified femur growth plates of rapamycin or solvent-treated *Tsc1*$^{f/f}$ and *Prx1-Cre; Tsc1*$^{f/f}$ mice. Scale bar, 200 μm.

I. The length of the femur growth plate of rapamycin or solvent-treated *Tsc1*$^{f/f}$ and *Prx1-Cre; Tsc1*$^{f/f}$ mice.

J. The thickness of the femur cortical bones of rapamycin or solvent-treated *Tsc1*$^{f/f}$ and *Prx1-Cre; Tsc1*$^{f/f}$ mice.

K. The width of the growth plates of rapamycin or solvent-treated *Tsc1*$^{f/f}$ and *Prx1-Cre; Tsc1*$^{f/f}$ mice.

L. The diameter of the chondrocytes of rapamycin or solvent-treated *Tsc1*$^{f/f}$ and *Prx1-Cre; Tsc1*$^{f/f}$ mice.

M. H/E staining of the joints of rapamycin or solvent-treated *Tsc1*$^{f/f}$ and *Prx1-Cre; Tsc1*$^{f/f}$ mice. Scale bar, 200 μm.

Figure S4. The phenotypes of *Prx1-Cre; Tsc1*$^{f/f}$ embryos and p1 pups and *Dermo1-Cre; Tsc1*$^{f/f}$ and *Osx-Cre; Tsc1*$^{f/f}$ adult mice, related to Figure 2 and 5.

A. The *Prx1-Cre; Tsc1*$^{f/f}$ E18.5 embryo skeleton appeared to be normal. The mutant and control embryos were stained with alizarin red and alcian blue. Scale bar, 200 μm.

B. The long bones of p1 *Prx1-Cre; Tsc1*$^{f/f}$ were similar in length as the control pups. N=4 mice.

C. H/E staining revealed that the *Prx1-Cre; Tsc1*$^{f/f}$ p1 pups showed normal joint. Scale bar, 200 μm.

D. Western blot showed that Tsc1 was deleted in the BM-MSCs of *Dermo1-Cre; Tsc1*$^{f/f}$ mice (left panel) and osteoblasts of *Osx-Cre; Tsc1*$^{f/f}$ mice (right panel). BM-MSCs were isolated from *Osx-Cre; Tsc1*$^{f/f}$ and were induced to differentiate into osteoblasts by 50 ng/ml of BMP2 for 5 days. The cells were collected and the cell samples were analyzed by western blot.

E. Normal body weights of *Dermo1-Cre; Tsc1*$^{f/f}$ mice (left panel) and *Osx-Cre; Tsc1*$^{f/f}$ mice (right panel) compared to their controls. N=4 mice.

F. Normal body lengths of *Dermo1-Cre; Tsc1$^{f/f}$* mice (left panel) and osteoblasts of *Osx-Cre; Tsc1$^{f/f}$* mice (right panel). N=4 mice.

G. HE staining of femur bones revealed that *Dermo1-Cre; Tsc1$^{f/f}$* mice (left panel) and *Osx-Cre; Tsc1$^{f/f}$* mice (right panel) showed normal growth plates. The right panel: the heights of the growth plates of *Osx-Cre; Tsc1$^{f/f}$* and control mice. Scale bars, 200 μm (left panel) and 50 μm (middle panel). N=3 mice

H. Immuno-staining for Col10 on femur sections of *Prx1-Cre; Tsc1$^{f/f}$* and control mice (upper panel). Bottom panel: quantitation data for the heights of the proliferation zone (PZ) (based on Fig. 4A) and hypertrophic zone (HZ) (based on Col10) and the total growth plate zone (based on Fig. S3H). Scale bar, 50 μm. N=3 mice

I. Trabecular bone numbers were increased in *Dermo1-Cre; Tsc1$^{f/f}$* mice and *Osx-Cre; Tsc1$^{f/f}$* mice. N=4 mice.

J. Trabecular bone thickness was not significantly altered in *Dermo1-Cre; Tsc1$^{f/f}$* mice or *Osx-Cre; Tsc1$^{f/f}$* mice. N=4 mice.

K. Trabecular bone separation was decreased in *Dermo1-Cre; Tsc1$^{f/f}$* mice. N=4 mice.

Figure. S5. *Prx1-Cre; Tsc1$^{f/f}$* mouse bones showed altered expression of *Rankl* and *Opg*. N=3 mice.

A. Immunohistochemistry staining for RANKL and OPG on femur sections of *Prx1-Cre; Tsc1$^{f/f}$*, *Dermo-Cre; Tsc1$^{f/f}$* and control mice, showing that RANKL was decreased whereas OPG was increased on *Prx1-Cre; Tsc1$^{f/f}$* mouse bones. Scale bar, 50 μm.

B. *Prx1-Cre; Tsc1$^{f/f}$* mouse bone marrow showed an increase in OPG and a decrease in RANKL levels. Femur and tibia bones were used for the assay. N=3 independent experiments.

C. Co-culture experiments showed that reduced synthesis of M-CSF by *Tsc1$^{-/-}$* MSCs compromised the proliferation of monocytes. *Tsc1$^{-/-}$* or WT MSCs were plated overnight and then normal monocytes were plated on top of the MSCs. These plates were treated with M-CSF (25 ng/ml) for 3 days and the pictures were taken

under microscope. Right panel: Quantitation data of total cells of 5 random views of three repeated results. Scale bar, 50 μm. N=3 independent experiments.

Figure S6. Rapamycin treatment largely rescued the bone mass phenotype of *LysM-Cre; Tsc1*$^{f/f}$ mice, related to Fig. 6.

Rapamycin was intraperitoneally injected into 3 week-old mutant and control mice at the dose of 3 μg/g body weight per day for 40 days. N=5 mice.

A. Western blot showed deletion of *Tsc1* led to mTOR activation in *LysM*+ monocytes (left panel) and *Ctsk*+ osteoclasts (right panel), leading to an increase in p-S6.
B. Micro-CT images of the femur bones of rapamycin (rapa) or solvent-treated *Tsc1*$^{f/f}$ and *LysM-Cre; Tsc1*$^{f/f}$ mice.
C. The BV/TV of femurs of rapamycin or solvent-treated *Tsc1*$^{f/f}$ and *LysM-Cre; Tsc1*$^{f/f}$ mice.

Figure S7. *Tsc1* ablation inhibited osteoclast differentiation and resorption activity by altering OC size and the number of actin ring-like structures, related to Fig. 6 and 7.

A. mTOR activation was suppressed when monocytes were induced to differentiate into osteoclasts by M-CSF and RANKL.
B. Deletion of *Tsc1* in *LysM*+ monocytes impeded osteoclast differentiation. WT and *Tsc1*$^{-/-}$ monocytes were induced to differentiate by M-CSF and RANKL. After 5 days, the number of nuclei in each TRAP positive cells were counted and presented. The experiments were repeated 5 times with 3 mice each.
C. *Tsc1*$^{-/-}$ osteoclasts showed normal levels of autophagy markers p62 and LC3.
D. The abnormal morphology of the osteoclasts on bone sections of *Ctsk-Cre; Tsc1*$^{f/f}$ and *LysM-Cre; Tsc1*$^{f/f}$ mice (upper panel) whereas osteoclasts looked normal in *LysM-Cre; Tsc1*$^{f/f}$mice (upper panel). Scale bar, 50 μm.
E. *LysM-Cre; Tsc1*$^{f/f}$ (left panel) and *Ctsk-Cre; Tsc1*$^{f/f}$mouse (right panel) femur sections showed a decrease in the number of actin ring-like structures at the bone surface. Scale bar, 50μm.

F. A diagram showing the multiple roles played by mTOR signaling in bone size and quality control.

Supplementary Experimental Procedures

Bone histomorphometry

Bone histomorphometry was performed on undecalcified sections. For dynamic histomorphometric analysis，mice received injections of calcein (20 mg/kg) at 8 and 2d prior to sacrifice. The femur was embedded in methyl methacrylate after dehydration and xylene treatment. Four-μm-thick sections were made using a hard tissue microtome (Leica Microsystems Nussloch GmbH). The sections were left unstained for measurement of double calcein labeling. For bone-specific parameters measurement, the slides were stained with Villanueva-Goldner's trichrome method. Images were taken and analyzed using the Olympus DP72 microscope (Olympus Microsystems). All parameters were measured using OsteoMeasure software (OsteoMetrics).

Bone three-point bending experiment

Three-point bending experiments were conducted on an equipment (Reger RGM-2020, China) using fixed femurs. The ends of the femurs were fixed on the machine pedestal in horizontal position with a 12 mm span. The probe continuously moved down at the speed of 1 mm/min to press the bone, which automatically stopped 1 min after the bone fractured. All the data were collected and analyzed with the software supplied by the manufacturer. Then Vernier caliper was used for measurement of femoral long axis, short axis and minor axis in the central part of trabecular thickness. Max load, yield stress, and elastic modulus were automatically calculated by the software provided by the manufacturer.

X-ray and micro-CT analysis

The whole-body and femurs radiographs were taken with the Cabinet X-Ray system (LX-60, Faxitron Bioptics) using a standardized setting (45Kv for 8s). Trabecular and cortical bone architecture were assessed in femurs employing a micro-computed tomography analysis (micro-CT) system (micro-CT 40, Scanco Medical) performed following protocols provided by the manufacturer.

Isolation and culture of BM-MSCs

Mice of 6-8 weeks of age were sacrificed by cervical dislocation, rinsed in 70%

(vol/vol) ethanol for 3 min. The femur and tibia bones were extracted and cleaned free of muscle. The bones were placed in a dish of sterile PBS on ice. The femur or tibia ends were cut and the bone marrow was flushed out with α-MEM using a syringe. This was repeated a few times until the bone looked pale. The cells were dispersed and filtered through a 70 μm mesh to remove any bone debris. The BM-MSCs were cultured in α-MEM containing 15% (vol/vol) FBS in the presence of 100 μg/ml penicillin and 100 μg/ml streptomycin at 37℃ with 5% CO_2 in a humidified chamber for 5 days. Then the nonadherent cells were washed out with PBS and the BM-MSCs were either directly used or frozen for future experiments.

Differentiation of BM-MSCs

For MSC differentiation assays, BM-MSCs were seeded at a density of $5x10^4$ cells/well in 12-well plates with complete medium. The next day, the cells were cultured in complete medium supplemented with 10 mM β-glycerol phosphate and 50 μg/ml ascorbic acid for 7-10 days, with the medium changed every 3 days. The cells were then washed with PBS, fixed in 4% paraformaldehyde for 30 min, and stained for ALP using an Alkaline Phosphatase Kit (Sigma) following the manufacturer's instructions. For mineralization assay, the cells were cultured for 14, 21, or 28 days, which were then rinsed with distilled water, stained in 5% (wt/vol) silver nitrate solution under ultraviolet light for 1h, washed three times with distilled water, and then added 500 μl 5% (wt/vol) sodium thiosulfate solution to stop the reaction.

For MSC adipocyte differentiation, MSCs were plated at a density of $1x10^5$ cells/well in a 12-well plate and cultured in α-MEM supplemented with 15% FBS, 100 nM dexamethasone, and 5 μM insulin for 2 weeks. The cells were then washed, fixed in 4% paraformaldehyde for 30 min, and stained with Oil-red-O solution. For chondrocyte differentiation, MSCs were seeded at a density of 1.6×10^7 cells/well in 5 μl droplets in the center of wells in a 12-well plate, cultured at in α-MEM supplemented with 15% FBS, 100 nM dexamethasone, 10 ng/ml TGF-β1，and 1 μM ascorbate-2-phosphate for 21 days. The cells were then washed with PBS, fixed in 4% paraformaldehyde for 30 min, and stained with 1% Alcian Blue solution (in 0.1N HCL) for 30min.

Isolation and differentiation of monocytes

The bone marrow cells were cultured in α-MEM containing 15% (vol/vol) FBS in the presence of 100 μg/ml penicillin and 100 μg/ml streptomycin) at 37℃ with 5% CO2 in a humidified chamber for 16 hrs. The nonadherent cells were harvested and seeded at a density of $1x10^6$ cells/well in a 96-well plate for TRAP staining or at a density of 3×10^7 cells/well in two 6-well plates to collect RNA and Protein. These cells were cultured in α-MEM containing M-CSF (50 ng/ml) and RANKL (100 ng/ml) for 5 days, and stained for TRAP using a TRAP-leukocyte kit (sigma).

TRAP staining

To stain osteoclast cultures after BM monocytes were induced to differentiate with RANKL and M-CSF, the cells were fixed in 4% PBS-buffered paraformaldehyde for 30 min, washed with PBS, and then stained with Leukocyte Acid Phosphatase kit (387A, Sigma-Aldrich) for 1h at 37 °C, following the manufacturer's instructions. Images were taken and analyzed using the Olympus DP72 microscope (Olympus Microsystems). TRAP+ multinucleated cells (>3 nuclei) were counted as osteoclasts.

To stain bone sections, tibiae and femur were dissected out, fixed in 4% PBS-buffered paraformaldehyde overnight at 4 °C, decalcified in 15% EDTA for 2 weeks and washed with distilled water. The samples were dehydrated in gradient alcohols, cleared with xylene, embedded in paraffin through the standard procedures. Four-μm-thick sections were cut using microtome (Lexica Microsystems Nussle GmbH). the bone sections were deparaffinized in xylene and rehydrated in gradient alcohols. The slides were then stained with the Leukocyte Acid Phosphatase kit (387A, Sigma-Aldrich) for 1h at 37°C according to the manufacturer's instructions. Images were taken using the Olympus DP72 microscope (Olympus Microsystems).

Resorption pit analysis

Bone marrow monocytes were induced to differentiate into osteoclasts in the presence of RANKL and M-CSF for 3 days. These differentiated osteoclasts were trypsinized off the plates and seeded onto the dentin slices for 5 more days. The dentin slices were washed with PBS and fixed in 2.5% glutaraldehyde, sonicated in 1N NaOH for 1 minute to remove cells, and stained with 1% toluidine blue solution

for 10 min at room temperature. Resorption pits on bone slice were observed and numbered in 20 random fields of vision under a microscope.

Quantitative PCR

Total RNA was extracted by using Trizol regent (invitrogen). The RNA was reverse transcribed using Transcriptor Universal cDNA Master (Roche) according to the manufacturer's instructions. Real-time PCR was performed using Fast Start Universal SYBR Green Master kit (Roche) using ABI Prism 7500 Sequence Detection System (Applied Biosystems). The relative levels of mRNA species were calculated using the delta-delta CT method. The expression of all the target genes was normalized to *GAPDH*. The primer sequences are listed below:

Pparγ Forward:5'-GGAAAGACAACGGACAAATCAC-3' Reverse:5'-TACGGATCGAAACTGGCAC-3'

Col1a1 Forward:5'-CCGGAAGAATACGTATCACC-3' Reverse:5'-ACCAGGAGGACCAGGAAGTC-3'

Osterix Forward:5'-TGAGGAAGAAGCCCATTCAC-3' Reverse:5'-ACTTCTTCTCCCGGGTGTG-3'

Runx2 Forward:5'-CCGGTCTCCTTCCAGGAT-3' Reverse:5'-GGGAACTGCTGTGGCTTC-3'

RankL Forward:5'-GGGAACTGCTGTGGCTTC-3' Reverse:5'-GATGGTGAGGTGTGCAAATG-3'

Opg Forward:5'-AGCTGCTGAAGCTGTGGAA-3' Reverse:5'-GGTTCGAGTGGCCGAGAT-3'

M-Csf Forward:5'-GGAGACCTCGTGCCAAATTA-3' Reverse:5'-TATCTCTGAAGCGCAAGGTG-3'

Sox9 Forward:5'-GGAGCTCGAAACTGACTGGAA-3' Reverse:5'-GAGGCGAATTGGAGAGGAGGA-3'

E-Cadherin Forward:5'-TCAGTTCCGAGGTCTACAC-3' Reverse:5'-CTTCAAATCTCACTCTGCCC-3'

DC-Stamp Forward:5'-TACGTGGAGAGAAGCAAGGAA-3' Reverse:5'-ACACTGAGACGTGGTTTAGGAAT-3

OC-Stamp Forward:5'-TGGGCCTCCATATGACCTCGAGTAG-3 Reverse:5'-TCAAAGGCTTGTAAATTGGAGGAGT-3'

Nfatc1 Forward:5'-TGGAGAAGCAGAGCACAGAC-3' Reverse:5'-GCGGAAAGGTGGTATCTCAA-3'

C-Fos Forward:5'-CGGGTTTCAACGCCGACTA-3' Reverse:5'-TTGGCACTAGAGACGGACAGA-3'

Actin Forward:5'-CGTGAAAAGATGACCCAGATCA-3' Reverse:5'-CACAGCCTGGATGGCTACGT-3'

Mmp9 Forward 5'-CTGGACAGCCAGACACTAAAG-3' Reverse 5'-CTCGCGGCAAGTCTTCAGAG-3'

Ctsk Forward 5'-GAAGAAGACTCACCAGAAGCAG -3' Reverse 5'-TCCAGGTTATGGGCAGAGATT-3'

Trap Forward 5'-TGTCATCTGTGAAAAGGTGGTC-3' Reverse 5'-ACTGGAGCAGCGGTGTTATG-3'

Ihh Forward 5'-CTCTTGCCTACAAGCAGTTCA-3' Reverse 5'-CCGTGTTCTCCTCGTCCTT-3'

Pthrp Forward 5'-CATCAGCTACTGCATGACAAGG-3' Reverse 5'-GGTGGTTTTTGGTGTTGGGAG-3'

Wnt5a Forward 5'-CAACTGGCAGGACTTTCTCAA-3' Reverse 5'-CATCTCCGATGCCGGAACT-3'

Immunohistochemical staining

Bone sections were deparaffinized in xylene and rehydrated in gradient alcohols, then permeabilized with 0.1% Triton X-100 for 20 min at room temperature. Antigen retrieval was performed in citrate buffer. After that, the slides were blocked with 1% goat serum (dissolved in PBS) for 20 mins, followed by addition of specific primary antibody overnight at 4°C. The next day, the slides were washed in PBS, incubated in

secondary antibody for 1h at 37°C, and washed in PBS before mounted. Images were taken and analyzed using the Olympus DP72 microscope (Olympus Microsystems). Anti-Ki67 (ab15580, Abcam) and p-S6 (CST, 2211l) antibodies were used in this study. Col2α1 (ab-196619) and Col10 (ab58632) antibodies were purchased from Abcam. Osterix antibodies (sc-393325), β-Catenin (sc-7199), Ext1 (sc-515144), and Ext2 (sc-514092) were purchased from Santa Cruz.

Western Blot

Total proteins were extracted from cells or tissues with TNEN buffer containing phosphatase and proteinase inhibitors. Total protein content was determined by the Bradford method (Bio-Rad assay). The samples were then subjected to sodium dodecyl sulfate-polyacrylamide gel electrophoresis (SDS-PAGE) followed by transfer onto nitrocellulose membranes. The proteins were detected with specific antibodies. Immunoreactivity was detected using a Western Chemiluminescent HRP Substrate Kit (Millipore). Membranes were imaged with FluorChem M system (Protein Simple). Antibodies against p-S6 (4587s), p-p38 (9211s), p38 (9212s), Smad4 (9515), p-Smad1 (9553s), Smad1 (9743s), NF-κB (4764s), p-Jnk (9251s), Jnk (9252), and p62 (8025s) were purchased from Cell Signaling Technology, and antibodies against β-Catenin (sc-7199), IκB (sc-945), Ext1 (sc-515144), Ext2 (sc-514092), Wnt5a (sc-365370), and Actin (sc-81178) were purchased from Santa Cruz.

Measurement of bone marrow OPG and RANKL

The bone marrow was taken from the femur and tibia bones of WT and control mice and was centrifuged for 5 minutes. The supernatant was collected and used to determine the levels of OPG and RANKL. Commercially available mouse OPG ELISA detection kit (BOSTER, EK0481) and RANKL ELISA detection kit (BOSTER, EK0843) were used for the measurements.